



Overview of Coupon Testing of an IM7/8552 Composite Required to Characterize High-Energy Impact Dynamic Material Models

*Brian P. Justusson and Matthew J. Molitor
Boeing Research and Technology, St. Louis, Missouri*

*Jeff S. Iqbal and Mostafa Rassaian
Boeing Research and Technology, Seattle, Washington*

*Trenton M. Ricks and Robert K. Goldberg
Glenn Research Center, Cleveland, Ohio*

NASA STI Program . . . in Profile

Since its founding, NASA has been dedicated to the advancement of aeronautics and space science. The NASA Scientific and Technical Information (STI) Program plays a key part in helping NASA maintain this important role.

The NASA STI Program operates under the auspices of the Agency Chief Information Officer. It collects, organizes, provides for archiving, and disseminates NASA's STI. The NASA STI Program provides access to the NASA Technical Report Server—Registered (NTRS Reg) and NASA Technical Report Server—Public (NTRS) thus providing one of the largest collections of aeronautical and space science STI in the world. Results are published in both non-NASA channels and by NASA in the NASA STI Report Series, which includes the following report types:

- TECHNICAL PUBLICATION. Reports of completed research or a major significant phase of research that present the results of NASA programs and include extensive data or theoretical analysis. Includes compilations of significant scientific and technical data and information deemed to be of continuing reference value. NASA counter-part of peer-reviewed formal professional papers, but has less stringent limitations on manuscript length and extent of graphic presentations.
- TECHNICAL MEMORANDUM. Scientific and technical findings that are preliminary or of specialized interest, e.g., “quick-release” reports, working papers, and bibliographies that contain minimal annotation. Does not contain extensive analysis.
- CONTRACTOR REPORT. Scientific and technical findings by NASA-sponsored contractors and grantees.
- CONFERENCE PUBLICATION. Collected papers from scientific and technical conferences, symposia, seminars, or other meetings sponsored or co-sponsored by NASA.
- SPECIAL PUBLICATION. Scientific, technical, or historical information from NASA programs, projects, and missions, often concerned with subjects having substantial public interest.
- TECHNICAL TRANSLATION. English-language translations of foreign scientific and technical material pertinent to NASA's mission.

For more information about the NASA STI program, see the following:

- Access the NASA STI program home page at <http://www.sti.nasa.gov>
- E-mail your question to help@sti.nasa.gov
- Fax your question to the NASA STI Information Desk at 757-864-6500
- Telephone the NASA STI Information Desk at 757-864-9658
- Write to:
NASA STI Program
Mail Stop 148
NASA Langley Research Center
Hampton, VA 23681-2199



Overview of Coupon Testing of an IM7/8552 Composite Required to Characterize High-Energy Impact Dynamic Material Models

*Brian P. Justusson and Matthew J. Molitor
Boeing Research and Technology, St. Louis, Missouri*

*Jeff S. Iqbal and Mostafa Rassaian
Boeing Research and Technology, Seattle, Washington*

*Trenton M. Ricks and Robert K. Goldberg
Glenn Research Center, Cleveland, Ohio*

National Aeronautics and
Space Administration

Glenn Research Center
Cleveland, Ohio 44135

Acknowledgments

The material in this report is based upon work supported by NASA under Award numbers NNL09AA00A and 80LARC17C0004. The authors gratefully acknowledge the technical contributions from the following: Matt Melis and Mike Pereira, NASA Glenn Research Center; Jenna Pang, Alan Byar, Brian Kasperson, and Mark Pankow, North Carolina State University.

This work was sponsored by the Advanced Air Vehicle Program
at the NASA Glenn Research Center

Trade names and trademarks are used in this report for identification
only. Their usage does not constitute an official endorsement,
either expressed or implied, by the National Aeronautics and
Space Administration.

Level of Review: This material has been technically reviewed by technical management.

Available from

NASA STI Program
Mail Stop 148
NASA Langley Research Center
Hampton, VA 23681-2199

National Technical Information Service
5285 Port Royal Road
Springfield, VA 22161
703-605-6000

This report is available in electronic form at <http://www.sti.nasa.gov/> and <http://ntrs.nasa.gov/>

Contents

1.0	Introduction.....	1
2.0	High-Energy Dynamic Impact Analysis Methods.....	3
3.0	Required Test Matrix.....	5
4.0	Test Results.....	8
4.1	Longitudinal Tension.....	8
4.1.1	Testing Details.....	8
4.1.2	Test Results.....	9
4.2	Transverse Tension.....	10
4.2.1	Testing Details.....	10
4.2.2	Test Results.....	11
4.3	In-Plane Shear.....	12
4.3.1	Testing Details.....	12
4.3.2	Test Results.....	12
4.4	Transverse Compression.....	13
4.4.1	Testing Details.....	13
4.4.2	Test Results.....	14
4.5	Through-Thickness Tension.....	16
4.5.1	Testing Details.....	16
4.5.2	Test Results.....	16
4.6	Out-of-Plane Shear (2-3 Direction).....	17
4.6.1	Testing Details.....	17
4.6.2	Test Results.....	18
4.7	Density Characterization.....	19
4.7.1	Testing Details.....	19
4.7.2	Test Results.....	19
4.8	Quasi-Static Punch Shear.....	20
4.8.1	Testing Details.....	20
4.8.2	Test Results.....	20
4.9	Out-of-Plane Off-Axis Compression.....	25
4.9.1	Testing Details.....	25
4.9.2	Test Results.....	25
4.10	Split Hopkinson Pressure Bar (SHPB).....	26
4.10.1	Testing Details.....	26
4.10.2	Test Results.....	26
4.11	Compact Compression.....	28
4.11.1	Testing Details.....	28
4.11.2	Test Results.....	28
4.12	Compact Tension.....	28
4.12.1	Testing Details.....	28
4.12.2	Test Results.....	28
4.13	Four-Point Bending.....	29
4.13.1	Testing Details.....	29
4.13.2	Test Results.....	29
4.14	Double Cantilever Beam (DCB).....	31

4.14.1 Testing Details	31
4.14.2 Test Results	32
4.15 End-Notched Flexure (ENF).....	33
4.15.1 Testing Details	33
4.15.2 Test Results	33
4.16 Mixed-Mode Bending (MMB)	35
4.16.1 Testing Details	35
4.16.2 Test Results	35
References.....	37

Overview of Coupon Testing of an IM7/8552 Composite Required to Characterize High-Energy Impact Dynamic Material Models

Brian P. Justusson and Matthew J. Molitor
Boeing Research and Technology
St. Louis, Missouri 63134

Jeff S. Iqbal and Mostafa Rassaian
Boeing Research and Technology
Seattle, Washington 98108

Trenton M. Ricks and Robert K. Goldberg
National Aeronautics and Space Administration
Glenn Research Center
Cleveland, Ohio 44135

Abstract

As part of NASA's Advanced Composites Project (ACP), a significant research effort was established to develop and mature analysis methods for composite materials particularly applicable to high-energy dynamic impact applications. An overall goal was to develop and advance analysis methods that can be characterized using fundamental coupon level tests. Based on this fundamental characterization, simulations at the higher levels of a building block approach can be purely predictive. The tests described in this report were performed on a unidirectional carbon fiber polymer matrix composite, IM7/8552 tape, as this material system is representative of a modern aerospace grade carbon fiber tape system. These tests were chosen to provide fundamental material characterization data for three representative progressive damage and failure analysis material models available within the LS-DYNA commercial transient dynamic finite element code for use in the simulation of the dynamic and impact response of composite materials. Two of the material models, MAT162 and MAT261, are well established material models within LS-DYNA. The third material model, MAT213, is under active development. Testing consisted primarily of ASTM-type standard tests, and the tests that were performed were consistent with the needs of all three models. Additionally, coupon level tests were performed that can be used to characterize a delamination model (e.g., cohesive zone or tie-break contact). While, the tests described in this report provide fundamental material characterization data for all three of the material models mentioned above, the data is applicable to additional material models not discussed.

1.0 Introduction

The NASA Advanced Composites Consortium (ACC) was a collection of industry, academic, and government subject matter experts who have worked in conjunction to develop and transition technology that will enable a reduction in the timeline required for development and certification of new aircraft structures that utilize advanced composite materials (Ref. 1). The ACC was a significant part of the NASA Advanced Composites Project (ACP). High fidelity analysis methods that can reliably predict the deformation, onset of damage, and damage progression in composite materials can contribute to this goal by replacing some of the testing requirements in the building block approach used for the design and

certification of primary aircraft structures (Ref. 2). Additionally, these analysis methods offer the potential for the development of design curves that can lead to more efficient structural concepts. The ACP project utilized a combination of experts from government, industry, and academia to develop and mature these high fidelity analysis methods. A significant subtask under ACP was to develop and mature analysis methods for composite materials particularly applicable to high-energy dynamic impact applications.

Within the development of a standard building block type approach for aircraft structures, modeling techniques are developed through inverse analysis of component or sub-component testing. The result of the current approach is predictive capability that is limited to the direct, or known, design space. The tools often lack flexibility to be used broadly across the design space. The ACC had an overall goal of an analysis method development effort aimed at creating techniques and algorithms that can be characterized using fundamental coupon level tests, as shown in the lowest level of the building block diagram shown in Figure 1. Based on this fundamental characterization, simulations at the higher levels of the building block can be purely predictive. In this report, the results of coupon testing are presented as the tests were designed specifically to characterize the high-energy dynamic impact analysis methods that were developed and utilized as part of the overall effort.

The tests described in this report were performed on a unidirectional carbon fiber polymer matrix composite, IM7/8552 tape (Ref. 3), as this material system is representative of a modern aerospace grade carbon fiber tape system.

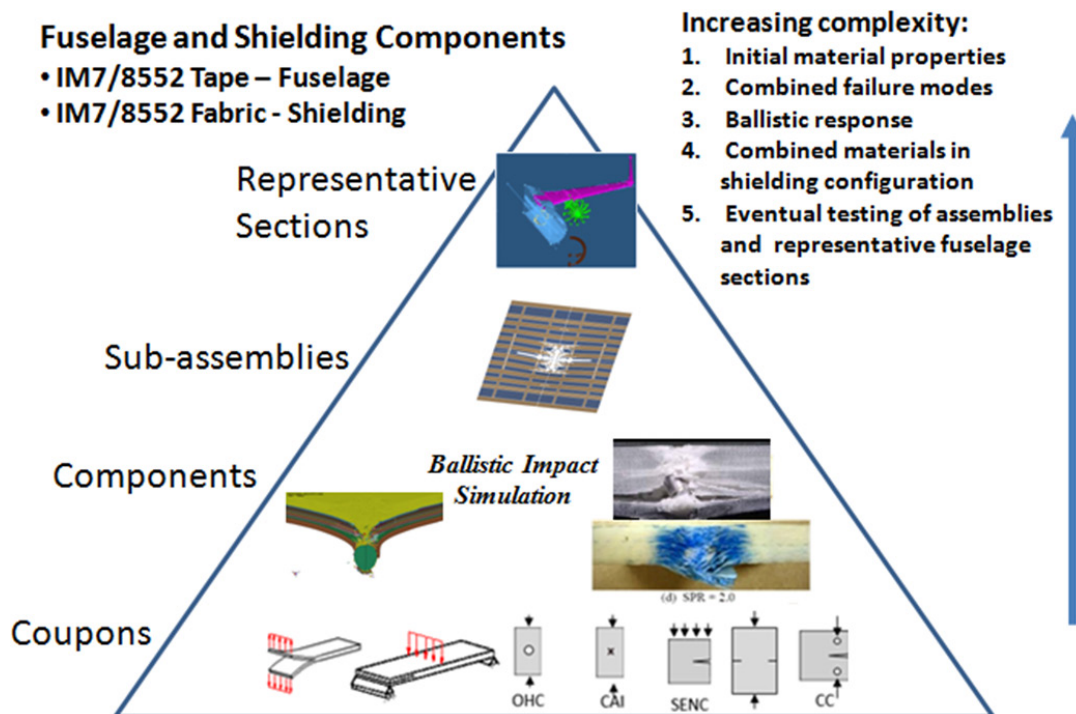


Figure 1.—Validation Building Block.

2.0 High-Energy Dynamic Impact Analysis Methods

The test results documented in this report were chosen to provide fundamental material characterization data for three representative progressive damage and failure analysis (PDFA) material models available within the LS-DYNA commercial transient dynamic finite element code for use in the simulation of the dynamic and impact response of composite materials. Two of the material models, MAT162 and MAT261, are well established material models within the LS-DYNA commercial transient dynamic finite element code (Ref. 4). The third material model, MAT213, is under active development by a team jointly led by the NASA Glenn Research Center and the Federal Aviation Administration. Testing consisted primarily of ASTM-type standard tests, and the tests that were performed were consistent with the needs of all three models. The specific emphasis in this report is on the material testing required to characterize the MAT213 material model described below. However, the tests described in this report will provide fundamental material characterization data for all three of the material models mentioned above, as well as additional material models not discussed here.

Each of these material models are constitutive models which describe the response of the material at a lamina (ply) or laminate scale with varying degrees of assumptions based on the material form and calibration parameters. The primary application is at the lamina scale to perform ply-by-ply modeling. The lamina scale offers a relevant length scale for the mechanics and is verifiable with experimental data. In this approach, each element is meant to represent multiple representative volume elements (RVEs) of the actual material form. For example, in a tape system, the RVE could be several hundreds of fibers within a matrix.

Commonly, the stress-strain response of polymer composites displays a noticeable amount of nonlinearity in one or more of the material directions after an initial linear (elastic) response. Within the finite element framework, a constitutive model can be developed that captures nonlinear characteristic responses through various numerical approaches. Specifically, the stress-strain response can be assumed to have the following components discussed below based on the model proposed by Razi (Ref. 5).

- a. *Elastic Response*: The elastic region is the initial linear region of the stress-strain curve. The strains are assumed to be completely recoverable. In general, it is best to characterize all nine elastic properties (assuming the material to be orthotropic at most) to give the highest confidence in the constitutive model. However, assumptions can be made to limit the necessary testing (e.g., transverse isotropy).
- b. *Pre-Peak Response*: The region of the stress-strain curve that displays nonlinearity but the stress levels are lower than the maximum stress is referred to as the pre-peak region. In general, this nonlinearity has been shown to have both elastic/recoverable nonlinearities due to deformation mechanisms as well as non-recoverable damage. The constitutive model of the pre-peak response ultimately governs how much energy is dissipated or recoverable.
- c. *Failure Criteria*: Comprehensive material models incorporate a number of failure modes that are characterized by failure parameters. In order to know that an element has failed, a relevant failure criteria is necessary for each mode of failure. Many methods have traditional matrix interaction failure criteria. However, during a high velocity impact, complex material interactions can occur, and it is more difficult to define appropriate failure criteria.
- d. *Post-Peak*: The post-peak response defines how energy is dissipated from a material after the failure criteria is met. The post-peak response can have one of three forms:
 1. Instantaneous energy degradation where energy is instantly removed from the system by element deletion or a similar method
 2. Energy based degradation where fracture like processes take place and dissipate the energy
 3. Calibrated energy dissipation where a post-peak softening curve is calibrated to one or more specific tests

An overview of the material models for which the coupon test data described in this report are intended to be used in the characterization process is presented below.

LS-DYNA MAT162

MAT162 is a composite material model in LS-DYNA for unidirectional and woven fabric materials for use with solid elements for perforation and penetration analyses. The material model is developed through the use of lamina level mechanics and models delamination through the inclusion of the originally developed S_DELM parameter. This parameter is not necessary when choosing to account for delamination discretely through the use of a tie-break constraint.

MAT162 requires testing for the standard orthotropic material properties, relevant strength parameters, and modeling considerations (e.g., nonstandard or calibrated material properties). The strengths and elastic properties are determined from ASTM-like standard testing. Some additional tests, not described in this report, are required to calibrate some of the specialized parameters in the material model.

LS-DYNA MAT261

The MAT261 model is similar to MAT162 in that it requires the elastic properties and strengths of the material and is a lamina level material model. It differs from MAT162 in that it uses an energy-based composite damage material model for solid and shell elements used in the LS-DYNA solver to model the composite laminate plies as opposed to MAT162 which requires calibration of material softening.

MAT261 requires testing for the standard orthotropic material properties, relevant strength parameters, and requires additional fracture based parameters to account for the energy dissipating mechanisms in the model. The strengths and elastic properties are determined from the same standard testing that is used for MAT162.

LS-DYNA MAT213

MAT213 is a composite material model in LS-DYNA suitable for use with solid or shell elements. The material model, which incorporates plasticity, damage, and failure, utilizes experimentally-based tabulated input to define the evolution of plasticity and damage and the initiation of failure as opposed to MAT162 and MAT261 which require only discrete input parameters such as modulus and strength. The plasticity portion of the composite constitutive model, utilized to simulate the nonlinear deformation response of the composite ply, is based on an extension of the Tsai-Wu composite failure model into a generalized yield function. For the damage model, employed to simulate the stiffness reduction and nonlinear unloading response observed in composites, a strain equivalent formulation is used to allow for the uncoupling of the deformation and damage analyses. For the failure model, a tabulated approach is utilized in which a stress- or strain-based invariant is defined as a function of the location of the current stress state in stress space to define the initiation of failure.

TABLE 1.—TEST MATRIX REQUIRED FOR FULL CHARACTERIZATION OF THE MAT213 MATERIAL MODEL

Test ID	Type
T1	Tension 1-direction
T2	Tension 2-direction
T3	Tension 3-direction
T4	Compression 1-direction
T5	Compression 2-direction
T6	Compression 3-direction
T7	Shear 1-2 plane
T8	Shear 2-3 plane
T9	Shear 1-3 plane
T10	Off-axis 45° 1-2 plane
T11	Off-axis 45° 2-3 plane
T12	Off-axis 45° 1-3 plane

To properly characterize MAT213, twelve standard coupon level tests (tension, compression, shear, and off-axis) in the various orthotropic material directions are required for solid finite element formulations, as specified in Table 1. The off-axis test data are used to control the rotation of the yield surface in a given plane and can be predicted if test data are unavailable. For each of these twelve tests, the entire stress-strain curve is provided in a tabulated form as input data, as opposed to point-wise values such as modulus and strength as is typically required for material model input. For shell finite element formulations, curves representing a 3-direction stress/strain response can be omitted. Delamination is not included as an integral part of MAT213. To model delamination, appropriate cohesive zone models or tie-break contact constraints need to be employed independently within a finite element model.

3.0 Required Test Matrix

For this study, the test matrix was developed by identifying the test methods required to populate the fundamental input properties of the three material models described above. It was split into multiple parts based on the level of applicability to the various material models. All of the tests were conducted or coordinated by Boeing. Table 2 shows the test matrix that is required to get standard elastic properties for any of the methods being implemented with 3D elastic criteria. These tests rely on ASTM-type standard test methods but also include Boeing proprietary methods that have been used in the past to determine improved properties. Table 3 shows some additional testing specifically required for population of the MAT162 and MAT213 material cards. Table 4 shows the required tests to generate the data to calibrate the tie-break contact definition within the LS-DYNA framework. As mentioned previously, the test matrix shown below only completely describes the material testing required to characterize, verify, and validate the MAT213 material cards and related delamination models. While the testing shown is also required for the MAT162 and MAT261 material cards, the complete test matrix required for the characterization of MAT162 and MAT261 will not be discussed within the context of this report. The purpose of this report is to fully document the fundamental data required to carry out verification and validation studies using MAT213 which will be described in future reports.

TABLE 2.—STANDARD TESTING TO DETERMINE ELASTIC PROPERTIES AND STRENGTHS

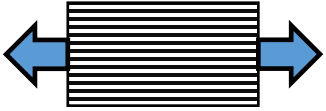
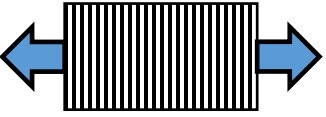
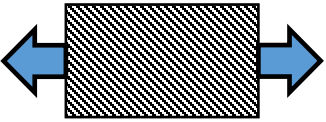
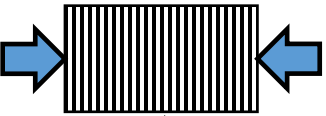
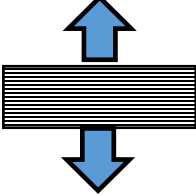
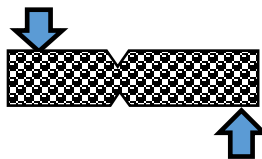
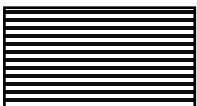
Test Type	Lay-up	Coupon Size	Quantity
Longitudinal Tension 	[90/0] _{2s}	10 in. x 1 in.	5
Transverse Tension 	[90] ₁₆	10 in. x 0.75 in.	5
In-Plane Shear 	[45/-45] _{2s}	10 in. x 1 in.	5
Transverse Compression 	[90] ₁₆	3.2 in. x 0.5 in.	5
Through-Thickness Tension 	[0] ₁₂₀	2 in. x 2 in.	10
Out-of-Plane Shear (2-3 Direction) 	[0] ₁₂₀	3.0 in. x 0.75 in.	10
Density Characterization 	[90] ₁₆	1 in. x 1 in.	5

TABLE 3.—REQUIRED SPECIALIZED TESTING FOR MODEL CHARACTERIZATION

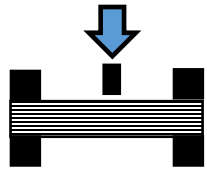
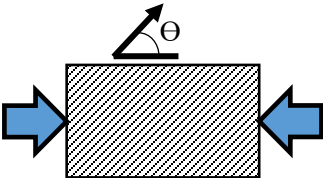
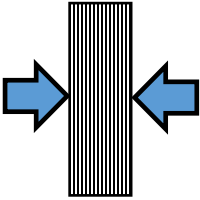
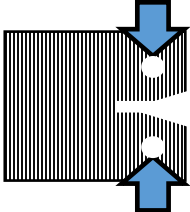
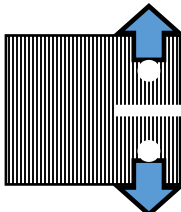
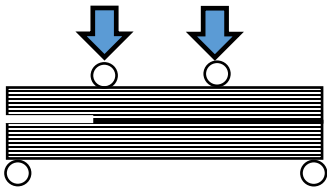
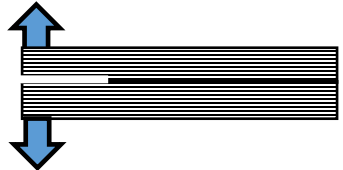
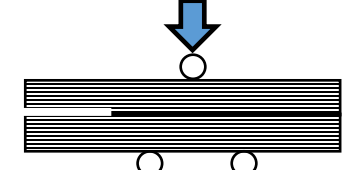
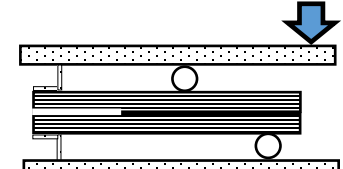
Test Type	Lay-up	Coupon Size	Quantity
<p>Quasi-Static Punch Shear</p> 	<p>$[0/90]_{24s} / [0/90]_{4s}$</p>	<p>8.0 in. x 8.0 in.</p>	<p>(5) – SPR = 0 (5) – SPR = 1.1 (5) – SPR = 2.0 (5) – SPR = 8.0</p> <p>20 Total</p>
<p>Out-of-Plane Off-Axis Compression</p> 	<p>$[0]_{120}$</p>	<p>0.59 in. x 0.59 in.</p>	<p>(5) – 0 deg (5) – 15 deg (5) – 30 deg (5) – 45 deg (5) – 60 deg (5) – 75 deg</p> <p>30 Total</p>
<p>Split Hopkinson Pressure Bar</p> 	<p>$[0]_{32} - C1$ $[90]_{32} - C2$ $[90]_{32} - C3$</p>	<p>0.5 in. x 0.5 in.</p>	<p>(15) – C1 Each (15) – C2 Each (15) – C3 Each</p> <p>45 Total</p>
<p>Compact Compression</p> 	<p>$[(90/0)_8/90/(0/90)_8]$</p>	<p>2.50 in. x 2.40 in.</p>	<p>5</p>
<p>Compact Tension</p> 	<p>$[(90/0)_5/90/(0/90)_5]$</p>	<p>2.50 in. x 2.40 in.</p>	<p>5</p>
<p>Four-Point Bending</p> 	<p>$[2/-2/0_9/-2/2/FEP/-2/2/0_9/-2/2]$</p>	<p>9 in. x 1 in.</p>	<p>10</p>

TABLE 4.—REQUIRED TESTING FOR TIE-BREAK CONTACT CALIBRATION

Test Type	Lay-up	Coupon Size	Quantity
<p>Double Cantilevered Beam</p> 	<p>[2/-2/0₉/-2/2/FEP/2/-2/0₉/-2/2]</p>	<p>10 in. x 1 in.</p>	<p>10</p>
<p>End Notch Flexure</p> 	<p>[2/-2/0₉/-2/2/FEP/2/-2/0₉/-2/2]</p>	<p>10 in. x 1 in.</p>	<p>10</p>
<p>Mixed-Mode Bending</p> 	<p>[2/-2/0₉/-2/2/FEP/2/-2/0₉/-2/2]</p>	<p>10 in. x 1 in.</p>	<p>(5) – MMR = 0.25 (5) – MMR = 0.50 (5) – MMR = 0.75 15 Total</p>

4.0 Test Results

The following sections describe the test techniques and test results for each of the experiments described in the previous section.

4.1 Longitudinal Tension

4.1.1 Testing Details

Samples were extracted from the bulk panel using a wet diamond coated tile saw and were inspected to be free of delamination. Testing was performed to be in accordance with SACMA RM9 standard (similar to the ASTM D3039 testing procedure). A total of five static tests were performed. A biaxial extensometer was installed on the specimen to measure the longitudinal and transverse strain in the sample.

The samples were loaded at a rate of 0.05 in./min. until ultimate failure was observed. Ultimate failure was defined as two piece failure or when the load dropped by 25 percent. The first coupon was tested until failure and the failure load was recorded. On the subsequent four (4) coupons, the samples were loaded to 90 percent of the failure load recorded previously. The load was then removed and the sample was loaded again at a rate of 0.05 in./min. until failure was observed. Upon completion of the test, a high resolution (10+ megapixel) image of the failed specimens, noting the specimen number for each test, was taken.

4.1.2 Test Results

The mechanical properties of the tape are shown in Table 5 which shows the stiffness, strength, and failure strain. The stiffness was determined from the taking the slope of the stress strain curve from a range of 2,000 to 5,000 microstrain. The strength was determined from taking the maximum value of stress and strain during the failure. Since the cross-ply tape specimens are balanced and symmetric laminates subjected to in-plane loads only, the only valid ply-level material property in the table is the strain to failure. Figure 2 shows the stress-strain response for the cross-ply tape system. The results are repeatable and generally consistent across the testing lots. Figure 3 shows the failure images for the tape. The samples failed in the gage section away from the grip locations as indicated by the discoloration near the sample ends.

TABLE 5.—MECHANICAL PROPERTIES FOR CROSS-PLY TAPE LAMINATE LOADED IN LONGITUDINAL TENSION

Specimen ID	Stiffness, msi	Strength, ksi	Failure strain, percent
P1-T-UNT-103-01	13.34	199.40	1.42
P1-T-UNT-103-02	13.42	202.32	1.46
P1-T-UNT-103-03	13.46	196.64	1.40
P1-T-UNT-103-04	13.26	203.30	1.47
P1-T-UNT-103-05	13.30	184.17	1.33
Average	13.36	197.17	1.42
Standard deviation	0.08	7.72	0.06

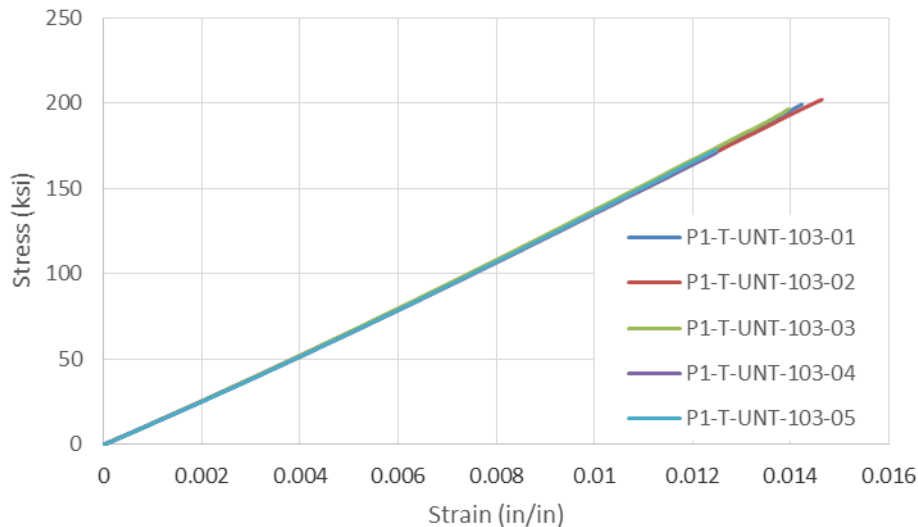


Figure 2.—Stress-Strain Longitudinal Tension Response of a Cross-ply Tape Laminate.



Figure 3.—Failed IM7/8552 Samples Subjected to Longitudinal Tension.

The cross-ply layup is used in the SACMA RM-9 standard to give a better indication of failure stress than what is determined from the ASTM D3039 specimen. ASTM D3039 calls for a unidirectional layup, which has been shown to be prone to splitting. By using a cross-ply layup, the splitting mode is suppressed by the transverse plies bridging the splitting fibers. To determine the equivalent unidirectional laminate strength, S_{11T} , from the measured cross-ply laminated strength, S_{11CP} , a backout factor, BF , is prescribed using lamina mechanics. The strength is as follows:

$$S_{11T} = S_{11CP} * BF$$

$$BF = \frac{2 * E_{11}}{E_{11} + E_{22}}$$

Assuming that the transverse plies have no stiffness due to crack saturation during loading, $BF = 2$, the average unidirectional strength under the longitudinal tension loading is 394.34 ± 15.44 ksi. Given these data and the fact that the response of the material is linear to failure in the longitudinal tension direction, the modulus (and stress-strain curve) of the unidirectional ply can be backed out. From the calculated average unidirectional strength and measured average failure strain, the unidirectional modulus can be estimated to be 27.77 ksi. This is somewhat larger than the 23.80 ksi modulus reported by Hexcel (Ref. 3).

4.2 Transverse Tension

4.2.1 Testing Details

In order to minimize the likelihood of introducing surface defects, the tape panel was covered in a protective coating (e.g., Teflon) on both surfaces after removal from autoclave processing. Samples were extracted from the bulk panel and inspected to be free of delamination. The coating was left intact during specimen extraction and removed only at the start of testing. All testing was performed in accordance with ASTM D3039 with the notable exception that the sample width was reduced to 0.5 in. A total of five (5) tests were performed. Failure was deemed acceptable if the specimens failed in the gage section away from the grips. Each sample had a biaxial extensometer applied to the sides of the specimen.

The samples were loaded under displacement control at a rate of 0.05 in./min. until ultimate failure was observed. Ultimate failure was defined as two-piece failure or when the load dropped by 25 percent. Upon completion of the test, a high resolution (10+ megapixel) image of the failed specimens, noting the specimen number for each test, was taken.

4.2.2 Test Results

The mechanical properties for the tape system are shown in Table 6. This table gives the stiffness, strength, and failure strain. The stiffness was determined from the taking the slope of the stress strain curve from a range of 2,000 to 5,000 microstrain. The strength (13.64±0.37 ksi) was determined from taking the maximum value of stress and strain during failure. Hexcel reports the transverse tensile strength to be 9.3 ksi (Ref. 3). This difference may be a result of the care that was taken with surface protection prior to testing. The stress-strain curves for the material system are shown in Figure 4.

The failed samples are shown in Figure 5. The samples displayed a cascade type fracture in which an initial fracture occurs, and the release of energy causes additional fractures to occur. Without the aid of high-speed photography, it is not possible to decipher the exact location of the initial fracture. Of note, coupon, P3-T-DYN-001-30 did not show any failure at the grips and had a single fracture path in the center of the coupon. Coupon P3-TDYN-001-032 had a single failure at the grips, however it had a higher strength. These results suggest that the testing is not sensitive to grip pressure or failure location and is representative of a material response and not the test setup.

TABLE 6.—MECHANICAL PROPERTIES OF THE TAPE SYSTEM IN TRANSVERSE TENSION

Specimen ID	Stiffness, msi	Strength, ksi	Failure strain, percent
P3-T-DYN-001-29	1.29	13.16	1.10
P3-T-DYN-001-30	1.30	13.32	1.11
P3-T-DYN-001-31	1.30	13.44	1.11
P3-T-DYN-001-32	1.29	14.22	1.20
P3-T-DYN-001-33	1.30	13.77	1.14
Average	1.29	13.58	1.13
Standard deviation	0.00	0.42	0.04

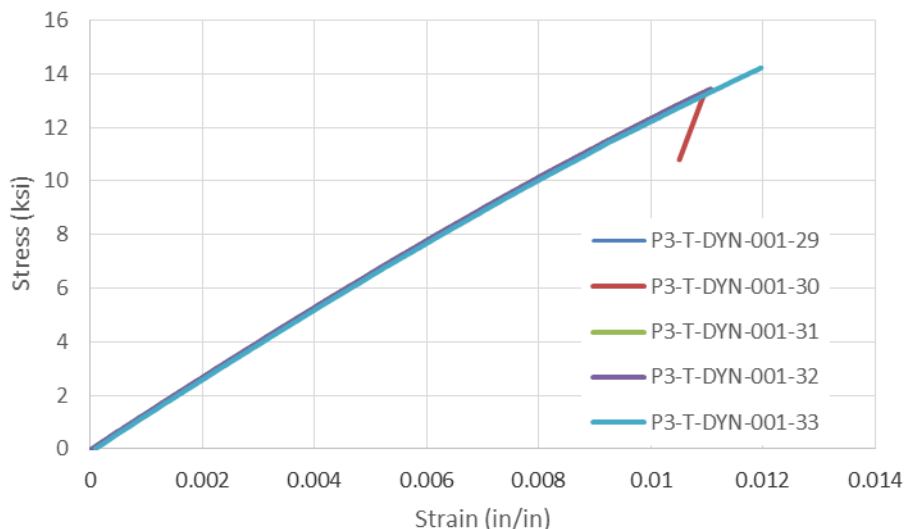


Figure 4.—Stress-Strain Transverse Tension Response.

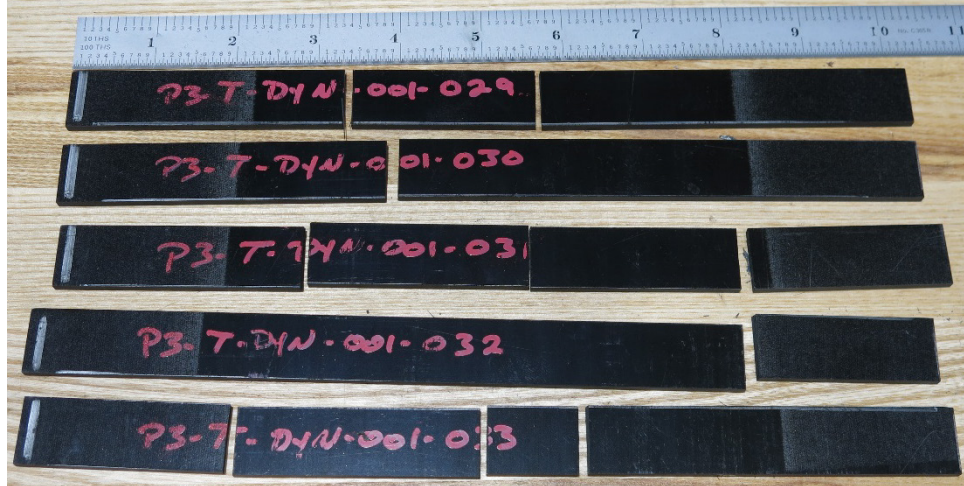


Figure 5.—Failed IM7/8552 Samples Subjected to Tension in the Transverse Direction.

4.3 In-Plane Shear

4.3.1 Testing Details

Samples were extracted from the bulk panel using a wet diamond coated tile saw and were inspected to be free of delamination via visual inspection. The cross-sectional area was measured from the coupon after sample preparation using a set of calipers for the width and a micrometer for the thickness. Testing was performed in accordance with the ASTM D3518 standard. A total of five (5) static tests were performed. A biaxial extensometer was attached to the side of the panel.

The samples were loaded at a rate of 0.05 in./min. until ultimate failure was observed. Failure was defined as the point in which 3 percent axial strain was achieved in the sample. When combined with the transverse strain to calculate a shear strain, this limit was beyond the point in which the ASTM standard defines failure as 5 percent shear strain. Upon completion of the test, a high resolution (10+ megapixel) image was taken of the failed samples.

4.3.2 Test Results

The mechanical properties (shear stiffness, shear strength, and failure strain) for the tape system are shown in Table 7. Of note, the failure strain is set by the ASTM standard which calls for the strength to be determined at 5 percent shear strain if the specimen has not failed.

To determine the shear stiffness, the experimental data needed to be processed into its related shear stress and shear strain components. From testing, the load, axial strain, and transverse strain were recorded. The shear stress was determined through a coordinate transformation as shown below:

$$\tau = \frac{\sigma}{2}$$

The shear strain was determined as follows:

$$\gamma = \epsilon_{\text{axial}} - \epsilon_{\text{transverse}}$$

The results of the coordinate transformation were used to generate the plots shown in Figure 6. The stiffness was determined by taking the slope of the line at from 1,000 to 3,000 microstrain to attempt to not capture any nonlinearity that may occur early during loading. The failure strength was determined by the stress in the coupon at 5 percent shear strain since no specimen had failed at that point.

TABLE 7.—MECHANICAL PROPERTIES FOR IN-PLANE SHEAR

Specimen ID	Stiffness, msi	Strength, ksi	Failure strain, percent
P2-T-UNT-103-01	0.69	12.73	5.00
P2-T-UNT-103-02	0.66	12.33	5.00
P2-T-UNT-103-03	0.65	11.90	5.00
P2-T-UNT-103-04	0.65	12.00	5.00
P2-T-UNT-103-05	0.67	12.28	5.00
Average	0.66	12.25	5.00
Standard deviation	0.02	0.33	0.00

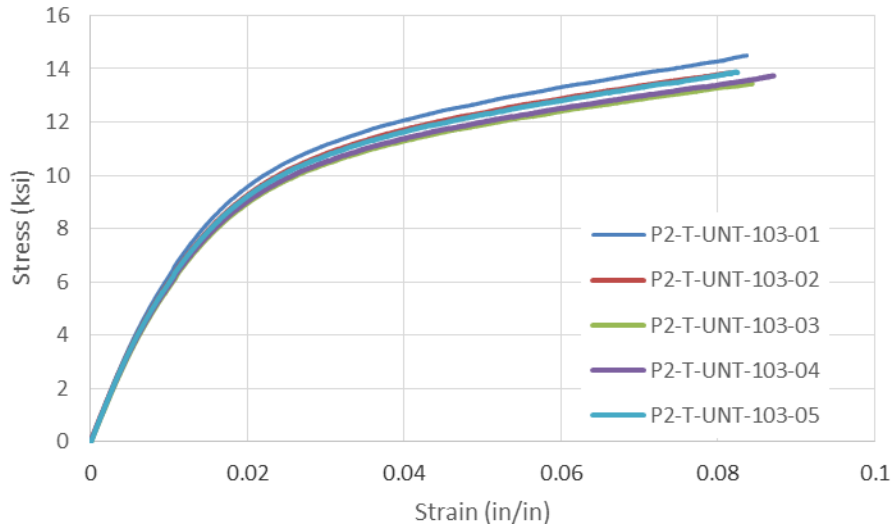


Figure 6.—Stress-Strain In-Plane Shear Response.

The coupons showed good repeatability with the failed samples shown in Figure 7. The tape samples when tested to failure showed a chevron type failure. This is consistent with a $\pm 45^\circ$ layup that is symmetric about the mid-plane.

4.4 Transverse Compression

4.4.1 Testing Details

The tape samples were tested in accordance with the ASTM D695 specification. A total of five (5) quasi-static tests were conducted. A side mounted extensometer was used and load was introduced via end loading as shown in Figure 8.

The sample was loaded at a rate of 0.05 in./min. until ultimate failure was observed. Ultimate failure was defined as two-piece failure or when the load dropped by 25 percent. Upon completion of the test, a high resolution (10+ megapixel) image of the failed specimens, noting the specimen number for each test, was taken.



Figure 7.—Failed IM7/8552 Samples Subjected to In-Plane Shear.

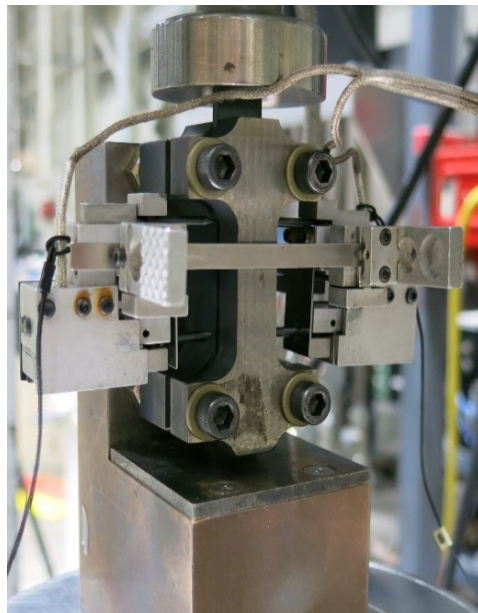


Figure 8.—Test Setup for Transverse Compression Testing of the IM7/8552 system.

4.4.2 Test Results

The mechanical properties for the tape system are shown in Table 8. Table 8 shows the transverse stiffness, the compressive strength, and the strain to failure for the material system. The modulus was determined by taking the slope of the stress-strain response from 2,000 to 4,000 microstrain for the material system, and the strength was determined from the peak load at which two piece failure was observed. The reported failure strain is the strain at which the peak strength was reached.

Figure 9 shows the stress strain response for the material system. The tape samples showed less than 10 percent difference in the strength, but this was most likely due to the nonlinearity observed in the sample as the error in the failure strain is much larger. This may most likely be due to the fact that the failure mode observed was not in the gage section, but rather on the loading end as shown in Figure 10.

TABLE 8.—MECHANICAL PROPERTIES FOR TRANSVERSE COMPRESSION

Specimen ID	Stiffness, msi	Strength, ksi	Failure strain, percent
P3-T-UNC90-103-01	1.40	39.74	3.93
P3-T-UNC90-103-02	1.39	47.37	4.98
P3-T-UNC90-103-03	1.35	39.32	3.69
P3-T-UNC90-103-04	1.63	39.69	3.16
P3-T-UNC90-103-05	1.50	41.85	3.63
Average	1.45	41.59	3.88
Standard deviation	0.11	3.38	0.68

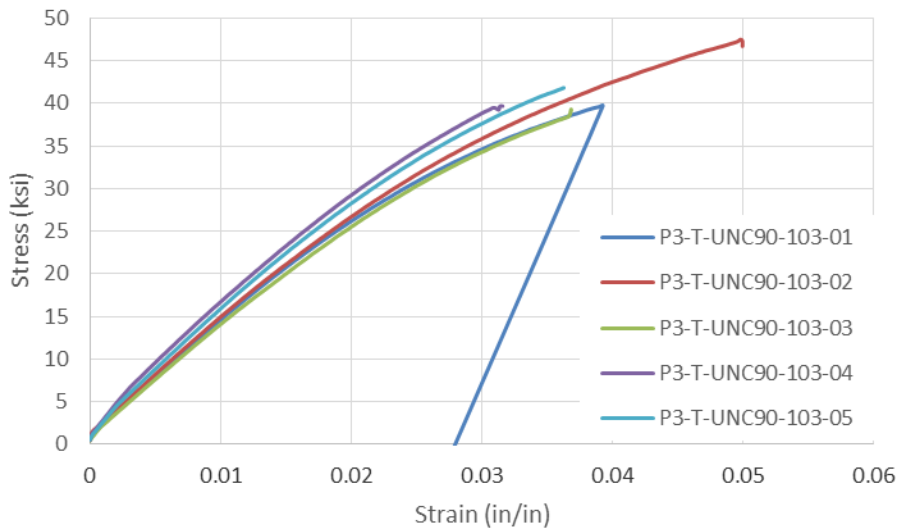


Figure 9.—Stress-Strain Transverse Compression Response.

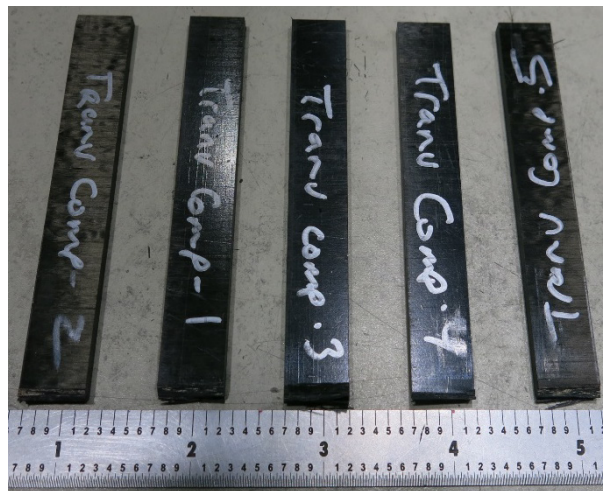


Figure 10.—Failed IM7/8552 Samples Subjected to Transverse Compression.

4.5 Through-Thickness Tension

4.5.1 Testing Details

Samples were extracted into 2 in. x 2 in. samples using a diamond coated wet saw and determined to be free of delamination. The samples were then cleaned of any oils and bonded to loading blocks. The blocks are compatible with the ASTM C297 fixture that is commercially available from Wyoming Test Fixtures (Wyoming Test Fixtures, Inc., Salt Lake City, UT). The cross-sectional area was measured from each coupon after sample preparation.

Four (4) samples were prepared with a random speckle suitable for digital image correlation (DIC) on the 1-3 face and four (4) samples were prepared with a random speckle suitable for DIC on the 2-3 face. 3D DIC was taken at a rate of one frame per second.

4.5.2 Test Results

The material properties generated from the testing are shown in Table 9. These properties include the elastic modulus, the tensile strength, the failure strain, and the Poisson's ratio. The stress was measured from the load cell data, and the strain was measured using an optical extensometer from the DIC data. The elastic modulus was determined by taking the slope of the stress-strain curve from 500 to 1,500 microstrain. The strength was determined from the maximum stress observed in the sample at two-piece failure; this value is not reported in Table 9 as additional samples were tested that did not include DIC. The strength of 5.85 ± 0.39 ksi is reported from other tests. This value is lower than what would be expected since the transverse tension strength was found to be 13.6 ksi. Failure was observed in the sample and not the adhesive. The DIC did not indicate any anomalies that would indicate premature failure.

The Poisson's ratios were determined from the DIC by using optical extensometers on the face of interest. Four stage points were created in the DIC analysis procedure as shown in Figure 11. The stage points were connected using a line and a 1-D description of the strain was generated using a simple Green's strain calculation. By taking the slope of the longitudinal strain (i.e., the measured strain in the loading direction) and transverse direction, the Poisson's ratio can be determined. Depending on which face is imaged, the 3-1 or 3-2 Poisson's ratio was determined. The measurements of the Poisson's ratios had low error.

TABLE 9.—MECHANICAL PROPERTIES FOR THROUGH-THICKNESS TENSION

Specimen ID	v31 (-)	v32 (-)	Stiffness, msi	Strength, ksi	Failure strain, percent
Tape-FWT-A-1	0.023	-----	2.10	-----	0.26
Tape-FWT-A-2	0.025	-----	2.10	-----	0.22
Tape-FWT-A-3	0.023	-----	2.02	-----	0.22
Tape-FWT-A-4	0.021	-----	1.67	-----	0.33
Tape-FWT-T-1	-----	0.380	1.35	-----	0.34
Tape-FWT-T-2	-----	0.361	1.53	-----	0.30
Tape-FWT-T-3	-----	*0.059	1.91	-----	0.23
Tape-FWT-T-4	-----	0.320	1.37	-----	0.33
Average	0.023	0.353	1.76	5.85	0.28
Standard deviation	0.002	0.031	0.32	0.39	0.05

*Denotes that the value was omitted from averaging calculations.

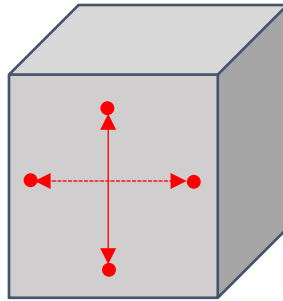


Figure 11.—Example of Optical Extensometers for DIC.

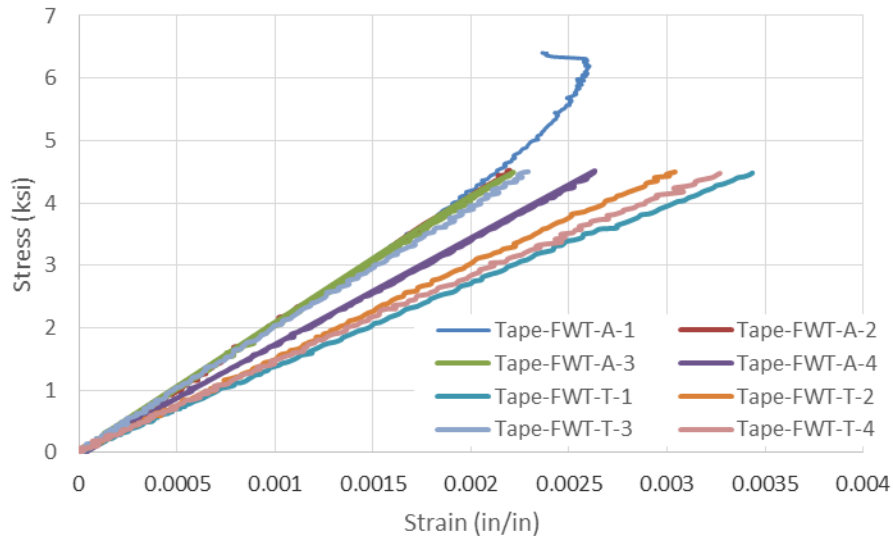


Figure 12.—Stress-Strain Response for Through-Thickness Tension.

The stress-strain response is shown in Figure 12. Of note, the stiffness varies significantly between samples. The elastic modulus was determined to be 1.76 ± 0.32 msi. The value was expected to be similar to that of the transverse tensile modulus (1.29 msi). The cause of the higher than expected result is not entirely known. However, the lower bound of the experimental error is reasonable when compared to the average transverse tensile modulus.

4.6 Out-of-Plane Shear (2-3 Direction)

4.6.1 Testing Details

The coupon geometry for out-of-plane shear in the 2-3 direction followed the ASTM D5379 standard for V-notched beam shear. Samples were inspected to be free of delamination. Each sample was prepared with a speckle pattern for DIC. The samples were loaded at a rate of 0.08 in./min. until ultimate failure was observed. Ultimate failure was defined as two-piece failure or when the load dropped by 25 percent. 3D DIC images were taken at a rate of one image per second.

4.6.2 Test Results

The out-of-plane shear stiffness and modulus are shown in Table 10. The results were generally repeatable as evidenced by the stress-tensorial shear strain curves shown in Figure 13. A near linear stress-strain response was measured for these tests.

TABLE 10.—MECHANICAL PROPERTIES FOR
OUT-OF-PLANE SHEAR TESTING

Specimen ID	Stiffness, msi	Strength, ksi
OOPS-Tape-1	0.33	8.42
OOPS-Tape-2	0.46	6.92
OOPS-Tape-3	0.34	9.20
OOPS-Tape-4	0.33	9.41
OOPS-Tape-5	0.39	7.68
Average	0.37	8.33
Standard deviation	0.06	1.04

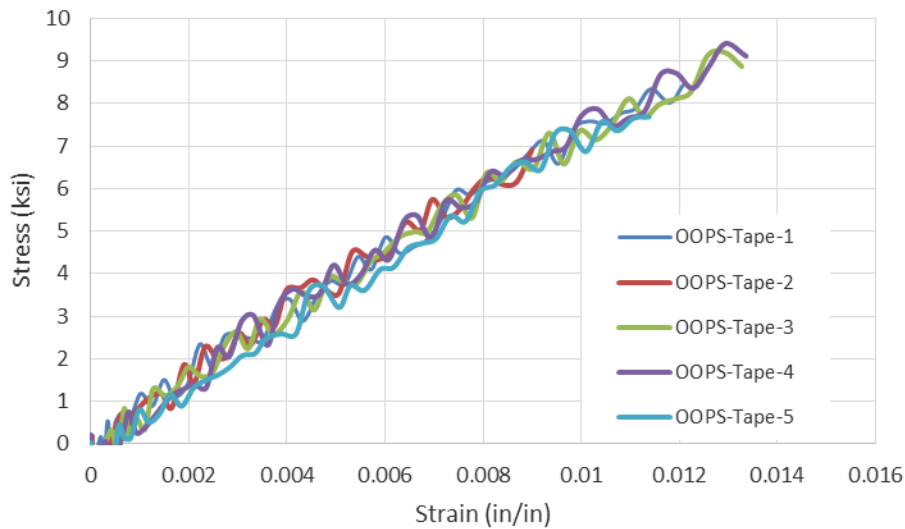


Figure 13.—Stress-Strain Response for Out-of-Plane Shear.

4.7 Density Characterization

4.7.1 Testing Details

Samples were extracted from the bulk panel using a diamond coated wet saw and were free of any delaminations. A total of eight (8) samples were tested in accordance with the ASTM D3800 Procedure A.

A beaker containing deionized water at room temperature was used and the weight of the sample was determined first in a dry state, and then when submerged in the water. The scale was tared for each measurement.

4.7.2 Test Results

Two measurements were used to determine the density of the tape: the dry weight ($W_{\text{dry wgt}}$) and the submerged (wet) weight ($W_{\text{wet wgt}}$). The buoyant force was determined by taking the difference between the dry weight and the wet weight and multiplying by the acceleration due to gravity, g , as shown below:

$$F_{\text{buoyant}} = (W_{\text{dry wgt}} - W_{\text{wet wgt}})g$$

The sample volume was determined from this by dividing the buoyant force by the density of the water:

$$\frac{F_{\text{buoyant}}}{\rho_{\text{water}}g} = \text{Sample Volume}$$

Using the dry weight as the mass and determined sample volume, the density of the material can be determined by dividing the mass by the volume. In total, eight (8) tape samples were used to determine the average density. It was determined that the density was 98.28 lb/ft³ for the tape as shown in Table 11.

TABLE 11.—DENSITY MEASUREMENTS FOR TAPE

Sample ID	$W_{\text{dry wgt}}$, oz.	$W_{\text{wet wgt}}$, oz.	ρ_{water} , oz./in. ³	F_{buoyant}/g , oz.	Sample volume, in. ³	Sample density, oz./in. ³
Tape #01	0.1080	0.0395	0.5766	0.069	0.119	0.910
Tape #02	0.1084	0.0398	-----	0.069	0.119	0.911
Tape #03	0.1078	0.0393	-----	0.069	0.119	0.908
Tape #04	0.1081	0.0396	-----	0.069	0.119	0.910
Tape #05	0.1084	0.0397	-----	0.069	0.119	0.910
Tape #06	0.1083	0.0395	-----	0.069	0.119	0.907
Tape #07	0.1085	0.0399	-----	0.069	0.119	0.912
Tape #08	0.1077	0.0395	-----	0.068	0.118	0.911
<i>Ave</i>	-----	-----	-----	<i>0.069</i>	<i>0.119</i>	<i>0.910</i>
<i>Average sample density, lb/ft³</i>						<i>98.280</i>

4.8 Quasi-Static Punch Shear

4.8.1 Testing Details

Samples were extracted from the bulk panel using a diamond coated wet saw and determined to be free of delamination. The cross-sectional area was measured from the coupon after sample preparation. Figure 14 shows a schematic of the QS-PST fixture. Of note, there are two critical dimensions: the punch diameter, D_p , and support span, D_s . The ratio of the support span to punch diameter is called the SPR. To determine the fiber crush strength, set $SPR = 0$. To determine the fiber shear strength, the SPR must be set to 1.1. A test matrix is shown in Table 12. The punch diameter was machined flat with no rounded edges. The sample was loaded at a rate of 0.05 in./min. via actuation of the punch. To determine the fiber crush strength, five (5) tests were performed with $SPR = 0$. This was achieved by using a backing plate, which created a condition in which the specimen is in pure compression. The specimen was loaded until ultimate failure (defined as the point in which the load dropped by 25 percent). For the SPR of 1.1, the sample was loaded until ultimate failure. Ultimate failure was defined in this case to occur when the punch penetrated through the sample. For the SPR of 2.0 and 8.0, it was necessary to generate data beyond the peak load with an additional displacement, δ . This displacement was used on subsequent tests and was determined independently for SPR of 2.0 and 8.0. Upon completion of the test, a high resolution (10+ megapixel) image of the failed specimens noting the specimen number for each test was taken.

4.8.2 Test Results

The first series of tests performed were for the $SPR = 0.0$ tests. This was performed in order to determine the crush strength of a ply that cannot be determined from a free compression test. The fixture was backed with a flat plate to not allow a span underneath the sample. A top plate with a span of 2 in. was placed on top of the test fixture and a punch of diameter 0.25 in. was used. The load deflection curves for the $SPR = 0.0$ are shown in Figure 15.

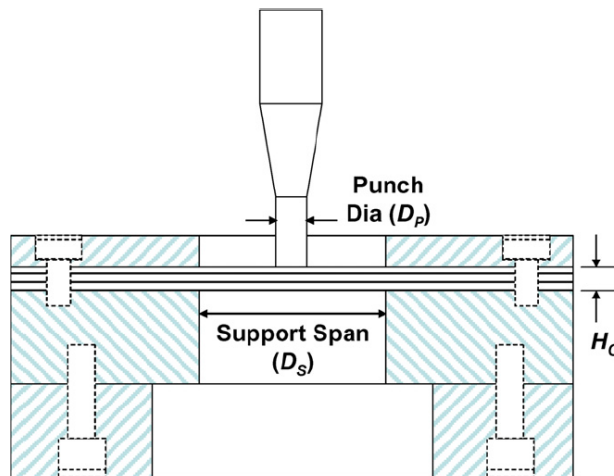


Figure 14.—Schematic of the Quasi-Static Punch Shear Test.

TABLE 12.—TEST MATRIX FOR QUASI-STATIC PUNCH SHEAR FOR TAPE

Layup condition	Specimen no.	D_p , in.	D_s , in.	SPR	Load level
[0/90] _{24s} (For SFC)	1	0.25	0	0	Ultimate
	2	0.25	0	0	Ultimate
	3	0.25	0	0	Ultimate
	4	0.25	0	0	Ultimate
	5	0.25	0	0	Ultimate
[0/90] _{24s} (For SFS)	1	1.8	2.0	1.1	Ultimate
	2	1.8	2.0	1.1	Ultimate
	3	1.8	2.0	1.1	Ultimate
	4	1.8	2.0	1.1	Ultimate
	5	1.8	2.0	1.1	Ultimate
[0/90] _{24s} (Thick)	1	1.0	2.0	2.0	Ultimate+ δ
	2	1.0	2.0	2.0	Ultimate+ δ
	3	1.0	2.0	2.0	Ultimate+ δ
	4	1.0	2.0	2.0	Ultimate+ δ
	5	1.0	2.0 </td <td>2.0</td> <td>Ultimate+δ</td>	2.0	Ultimate+ δ
[0/90] _{4s} (Thin)	1	0.5	4.0	8.0	Ultimate+ δ
	2	0.5	4.0	8.0	Ultimate+ δ
	3	0.5	4.0	8.0	Ultimate+ δ
	4	0.5	4.0	8.0	Ultimate+ δ
	5	0.5	4.0	8.0	Ultimate+ δ

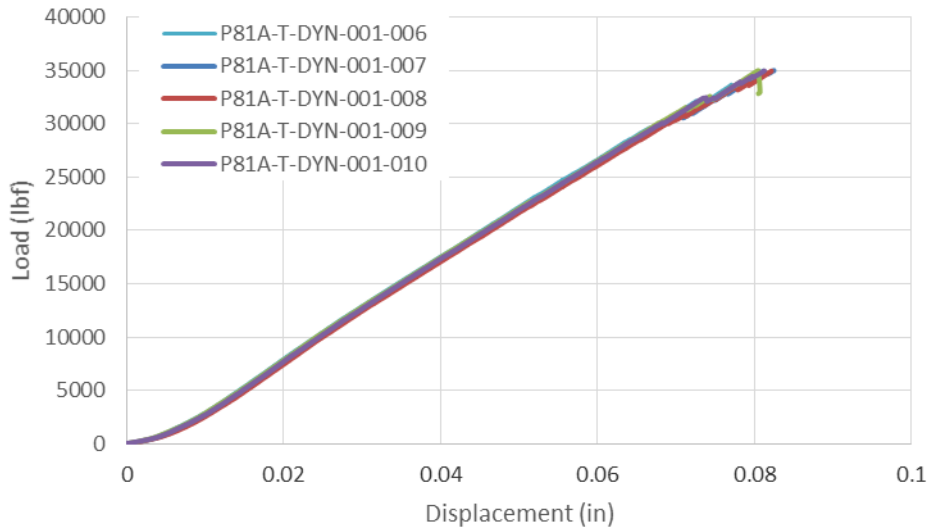


Figure 15.—Load-Displacement Curves for the Quasi-Static Punch Shear Test with SPR = 0.0.

Figure 15 for the tape system does not show a clear load drop. However, this behavior is expected as a hydrostatic state of stress is developed underneath the loading head. During the loading, there were characteristic small load drops that are consistent with an individual ply failing. After each of the load drops, the panel continued to be loaded. The final damage state is shown in Figure 16.

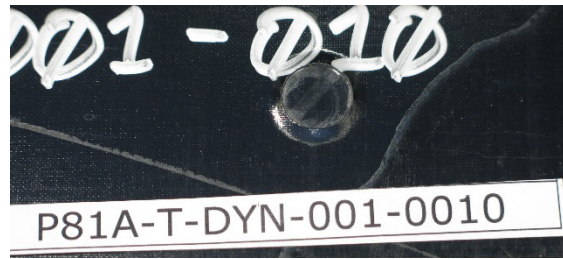


Figure 16.—Tested Sample for the Quasi-Static Punch Shear Test with SPR = 0.0.

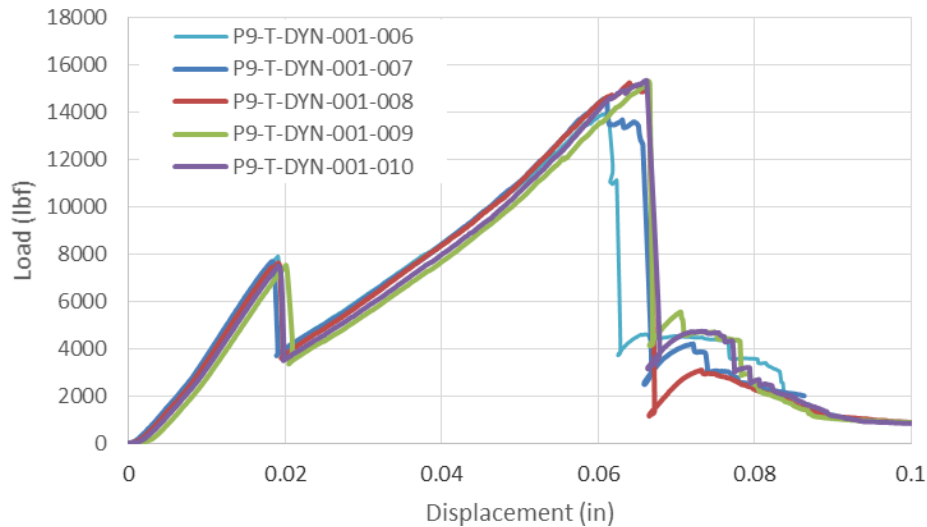


Figure 17.—Load-Displacement Curves for the Quasi-Static Punch Shear Test with SPR = 1.1

The next series of tests performed were for the SPR = 1.1 tests. This SPR ratio was used to determine the strength of the ply by shearing through the thickness. This result is different from that obtained in the through thickness shear test. The QSPST fixture was backed with a flat plate with a circularly opening of 2.0 in. The punch had a diameter of 1.8 in. The load deflection curves for the SPR = 1.1 are shown in Figure 17. Within these curves, there are two points of interest. The first is a characteristic load drop for the tape system that occurs at a displacement of 0.02 in. This load drop is a result that of an internal delamination. After that delamination forms, the plies begin to shear further until the final large load drop is observed. The load drop is consistent with a shear plug being developed and pushed through the surface. Figure 18 shows the sample after failure. From this, it is clear that there is a delamination that occurs internally as there is a lip of material that occurs. After failure, the plug pushes all the way through the sample.

At the completion of the test, the thickness of the lip was measured three (3) times using a micrometer. This allowed for determination of the depth of the delamination of as a result of the punch shear testing. These measurements were averaged and the result is shown in Table 13.

The next series of tests performed were for the SPR = 4.0 tests. This SPR ratio is used to determine a characteristically thick response. The QSPST fixture was backed with a flat plate with a circularly opening of 2.0 in. The punch had a diameter of 0.5 in. The load deflection curves for the SPR = 4.0 are shown in Figure 19.

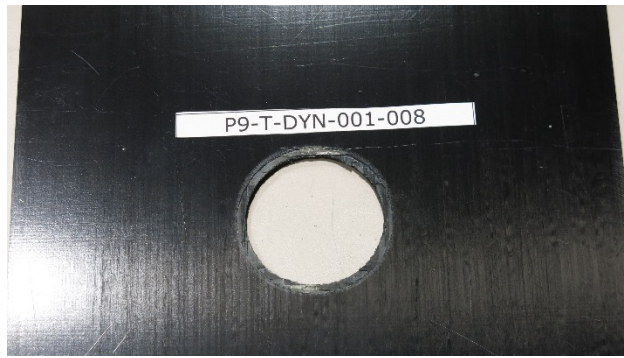


Figure 18.—Tested Sample for the Quasi-Static Punch Shear Test with SPR = 1.1.

TABLE 13.—THICKNESSES OF LIP DEVELOPED AS A RESULT OF DELAMINATION

Coupon	SPR	LIP thru thickness, in.			Average
		1	2	3	
P9-T-DYN-001-006	1.1	0.0505	0.0460	0.0510	0.0492
P9-T-DYN-001-007	1.1	did not punch out			-----
P9-T-DYN-001-008	1.1	0.0540	0.0430	0.0480	0.0483
P9-T-DYN-001-009	1.1	0.0525	0.0595	0.0485	0.0535
P9-T-DYN-001-0010	1.1	did not punch out			-----
P3A-2-F-DYN-001-006	1.1	0.0750	0.0775	0.0750	0.0758
P3A-2-F-DYN-001-007	1.1	0.0745	0.0800	0.0735	0.0760
P3A-2-F-DYN-001-008	1.1	0.0670	0.0640	0.0715	0.0675
P3A-2-F-DYN-001-009	1.1	0.0805	0.0755	0.0845	0.0802
P3A-2-F-DYN-001-0010	1.1	0.0545	0.0675	0.0545	0.0588

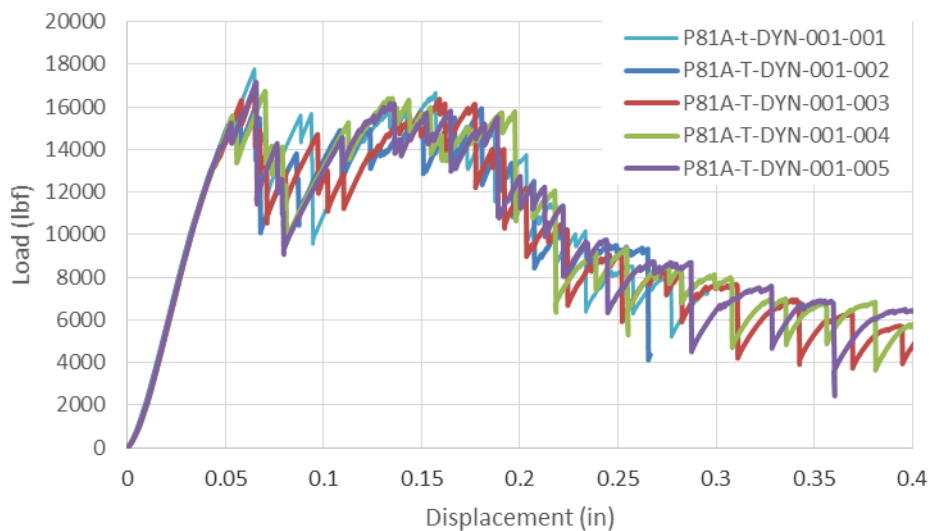
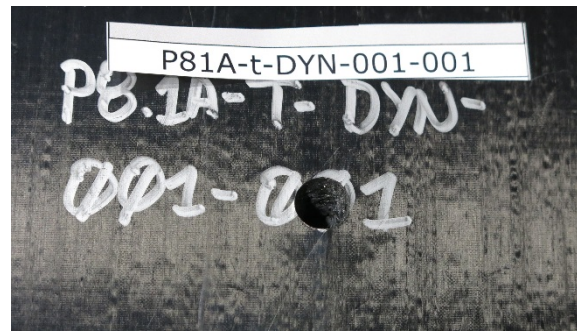


Figure 19.—Load-Displacement Curves for the Quasi-Static Punch Shear Test with SPR = 4.0.

The failed samples are shown in Figure 20. On the front face of the tape samples, the punch damaged the material through a shearing behavior. No additional damage was observed around the hole (e.g., splitting). On the back side of the sample, no complete perforation was observed.

The next series of tests performed were for the $SPR = 8.0$ tests. This SPR ratio was used to determine a characteristically thin response. The QSPST fixture was backed with a flat plate with a circular opening of 4.0 in. The punch had a diameter of 0.5 in. The load deflection curves for the $SPR = 8.0$ are shown in Figure 21.



(a) Front view



(b) Back view

Figure 20.—Tested Samples for the Quasi-Static Punch Shear Test with $SPR = 4.0$.

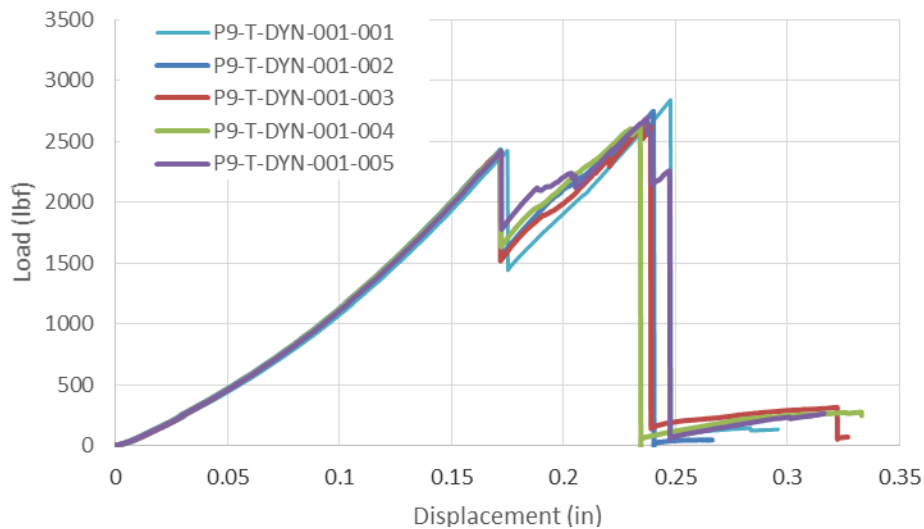
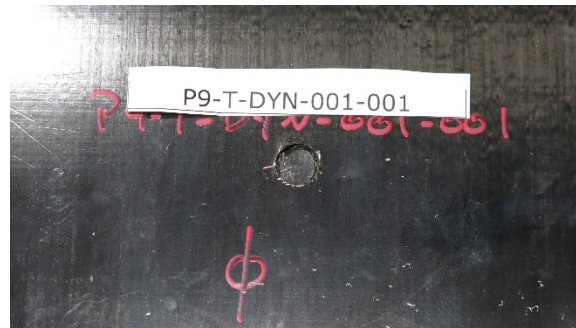
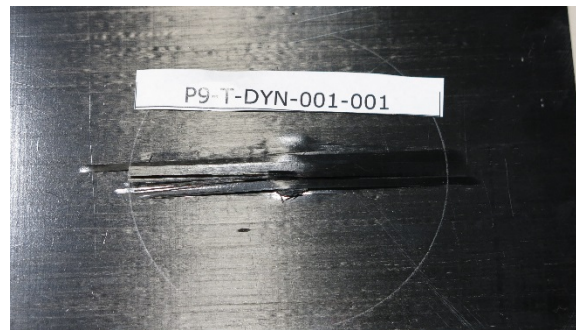


Figure 21.—Load-Displacement Curves for the Quasi-Static Punch Shear Test with $SPR = 8.0$.



(a) Front view



(b) Back view

Figure 22.—Tested Samples for the Quasi-Static Punch Shear Test with SPR = 8.0.

The failed samples are shown in Figure 22. On the front face of the tape samples, the punch damaged the material through a shearing behavior. No additional damage is observed around the hole (e.g., splitting) on the tape. After some appreciable loading, a delamination develops and begins to push through the samples. On the back side of the sample, no complete perforation was observed. However, splitting did occur.

4.9 Out-of-Plane Off-Axis Compression

4.9.1 Testing Details

Samples were extracted into 0.59 in. x 0.59 in. x 0.59 in. cubes from the bulk laminate using a CNC Zimmerman. The specimen were placed under a flat plate compression loading fixture. The samples were loaded at a rate of 0.05 in./min. until ultimate failure was observed. Ultimate failure was defined as two-piece failure. The test was performed with five (5) samples for each angle. Angles of 0°, 15°, 30°, 45°, 60°, and 75° were tested.

4.9.2 Test Results

Representative load-displacement curves are shown in Figure 23. In general, larger angles gave a softer load-displacement response as would be expected for a tape material system.

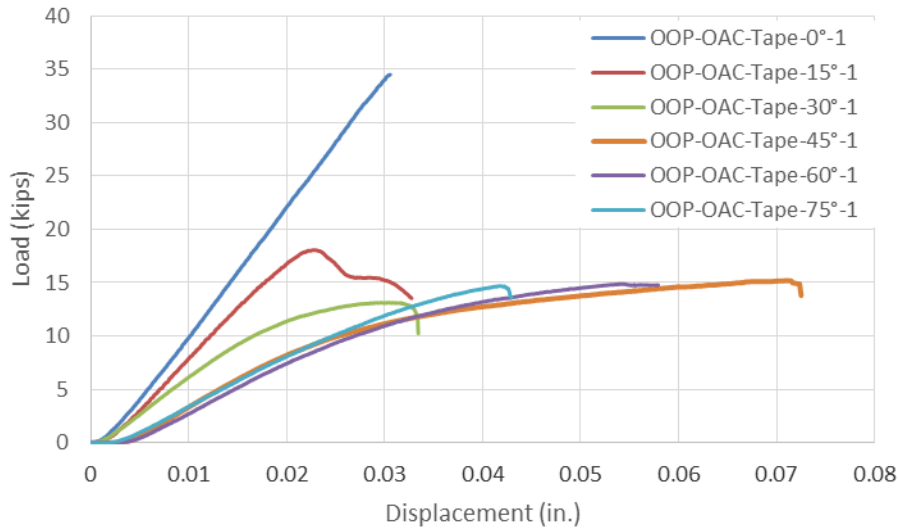


Figure 23.—The Load-Displacement Response for the Out-of-Plane Off-Axis Compression Tests for IM7/8552.

TABLE 14.—QUALITATIVE RESULTS FOR STRAIN RATE DEPENDENT EFFECTS

Material	Direction	Modulus	Strength
IM7/8552	Axial	No	No
	Transverse	Yes	Yes
	Through thickness	Yes	Yes

4.10 Split Hopkinson Pressure Bar (SHPB)

4.10.1 Testing Details

Samples were extracted from the bulk panel using diamond coated wet saw and then subjected to an additional grinding step to ensure the flatness and parallelness requirements of the material. Samples were inspected and determined to be free of delamination. The cross-sectional area was measured from the coupon after sample preparation.

A 0.75 in. Split Hopkinson Pressure Bar (SHPB) setup was used for high strain rate testing. The bars were made of maraging steel and allowed to move freely on linear bronze bearings. Firing pressures were targeted based on maximizing the pressure in the gas gun. Samples were prepared with a random speckle pattern and imaged at a framing rate of 100,000 frames per second.

Fifteen (15) samples were tested over a range of striker bar velocities to produce the necessary data. This procedure was repeated for each of the three principle material directions. The stress-strain response was generated from bar signals in a manner similar to that described in Koerber et al. (Ref. 6).

4.10.2 Test Results

A qualitative description of the test results is shown in Table 14. Modulus strengthening effects were observed in the transverse and through thickness response for the IM7/8552 system. Similarly, increases in strengths were observed for all orientations except the axial response for the IM7/8552. While strengthening may occur, compressive failure was not observed with delamination being the favorable mode of failure. In general, the results are consistent with the notion of the matrix showing strain rate dependence and fiber being strain rate independent.

The data was processed from the bar strains to produce dynamic stress-strain curves. An example of the stress-strain response is shown in Figure 24.

From the dynamic stress-strain curves, the modulus of elasticity and the strength were determined for each curve. The modulus was determined by taking the slope of the stress-strain curve from 2,000 to 5,000 micro-strain. The strength is determined from the maximum stress observed in the sample from failure. The dimensionless strain was determined by normalizing the strain rate by the static strain rate. For the examples shown in Figure 24, this is a strain rate of 0.00015/s for the transverse compression of the tape. In order to further analyze the data in dimensionless space, the strength and modulus were normalized by the static strengths.

To determine the strain rate effects, the dimensionless mechanical properties were plotted against the dimensionless strain rate. A logarithmic fit was used and the values are shown in Figure 25.

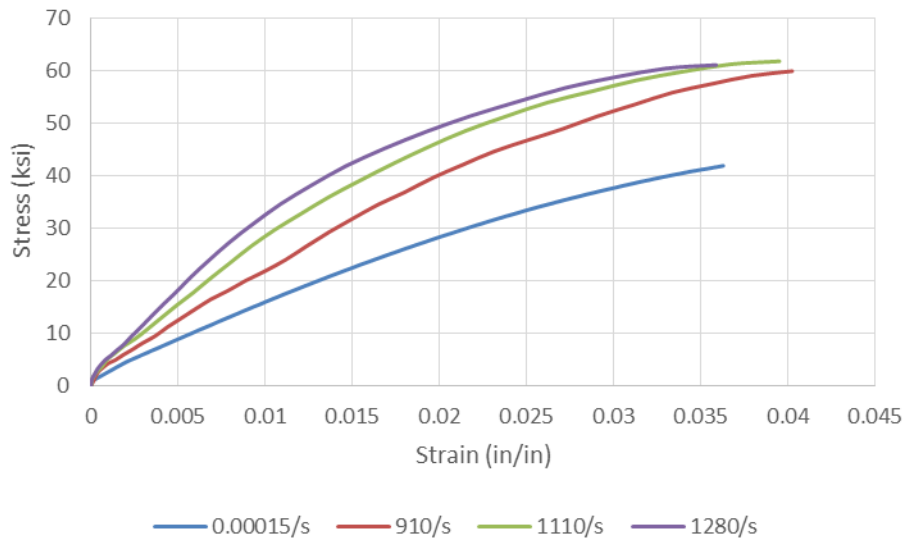


Figure 24.—Dynamic Stress-Strain Curves for the Transverse Compression Response of IM7/8552.

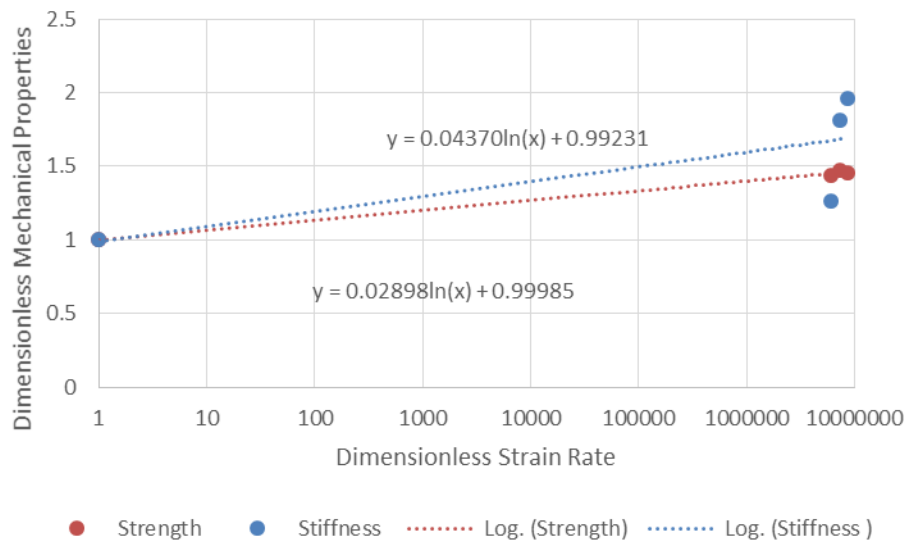


Figure 25.—Mechanical Properties for Dimensionless Strain Rates.

4.11 Compact Compression

4.11.1 Testing Details

Samples were extracted from the bulk panel using a CNC controlled Zimmerman and were inspected to be free of delamination. Any samples with discernible delamination(s) were not used for testing. A notch and the loading holes were placed in the center of the coupon from the CNC controlled Zimmerman program. Load was introduced into the sample via loading pins inserted into the holes in the sample. The sample was loaded at a rate of 0.05 in./min. until ultimate failure was observed. Ultimate failure was defined as when the load dropped by 80 percent of the peak strength. The DIC images were taken at a framing rate of one (1) frame per second.

4.11.2 Test Results

This test is in support of determining the fracture toughness of a fiber in compression. This fracture toughness property is not determined directly as a result of testing. However the load-deflection data can be used in concert with an inverse analysis approach to determine this property. The load-deflection curves are shown in Figure 26.

4.12 Compact Tension

4.12.1 Testing Details

Samples were extracted from the bulk panel using a CNC controlled Zimmerman and were inspected to be free of delaminations. Any samples with discernible delamination(s) were not used for testing. A notch and the loading holes were placed in the center of the coupon from the CNC controlled Zimmerman program. Load was introduced into the sample via loading pins inserted into the holes in the sample. The sample was loaded at a rate of 0.05 in./min. until ultimate failure was observed. Ultimate failure was defined as when the load dropped by 80 percent of the peak strength. The DIC was taken at a framing rate of one (1) frame per second.

4.12.2 Test Results

This test is in support of determining the fracture toughness of a fiber in compression. This property is not determined directly as a result of testing. However, the load-deflection data can be used in concert with an inverse analysis approach to determine this property. The load-deflection curves are shown in Figure 27.

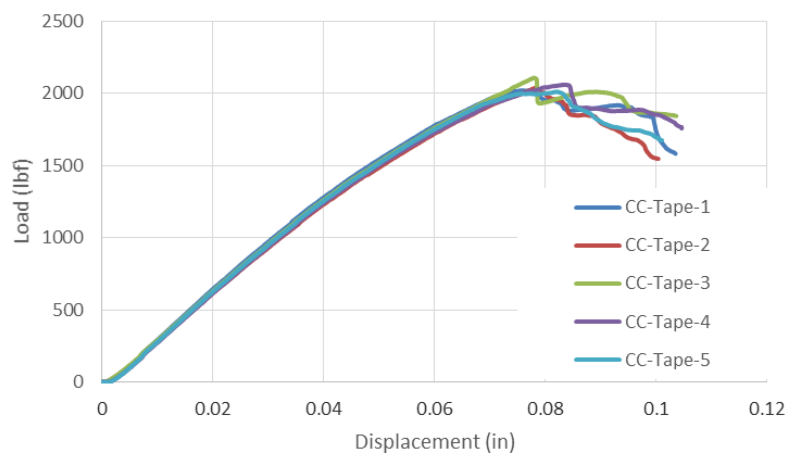


Figure 26.—Load-Deflection Response for Compact Compression (CC) Tests.

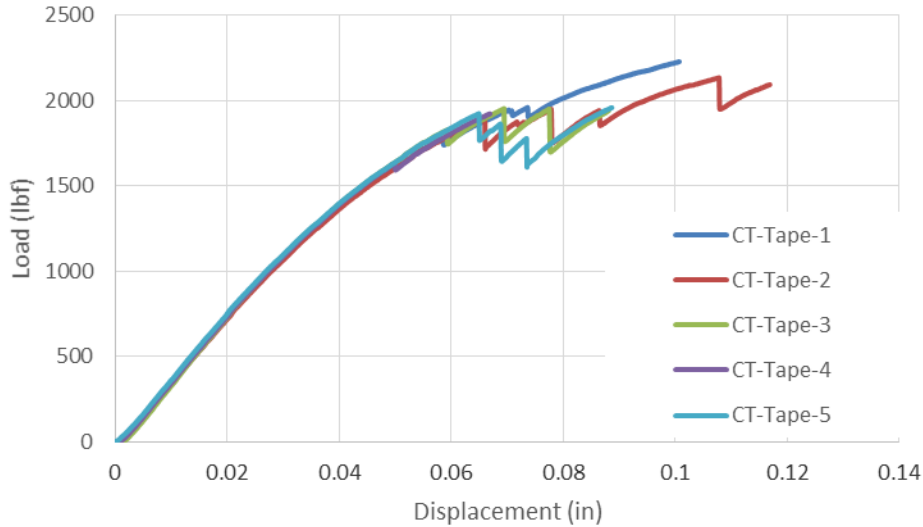


Figure 27.—Load-Deflection Response for Compact Tension (CT) Tests.

4.13 Four-Point Bending

4.13.1 Testing Details

Samples were cured with a 3 in. Teflon insert placed at the panel midplane to serve as a pre-crack in the panel. Samples were extracted from the bulk panel using diamond coated wet saw and were inspected to be free of delamination. The cross-sectional areas were measured from the coupon after sample preparation.

The test configuration is shown in Figure 28. The bottom rollers had a diameter of 1 in. and the bottom two rollers had a diameter of 0.5 in. The test had a span of 8 in. and was centered in the specimen. The top rollers were centered on the midpoint of the specimen and had a span of 4 in. The sample was loaded under displacement control at a loading rate of 0.002 in./s. and the deflection was measured with a deflectometer positioned underneath the loading head. Prior to testing, the side of the sample was painted white such that the final crack length could be measured (Figure 29).

4.13.2 Test Results

The four-point bend specimen can be used to determine the Mode II energy release rate, similar to what is produced by end-notched flexure (ENF) testing. Through traditional analysis, the fracture energy can be determined by the following equation:

$$G_{IIC} = \frac{mP^2}{2b}$$

where m is the slope of the compliance curve, P is the applied load, and b is the specimen width. The slope of the compliance curve was determined to be 0.000064/lb for the IM7/8552 system. The load-deflection curves are shown in Figure 30. In general, the four-point bend testing did not give as consistent of a result as the ENF testing for the Mode II fracture toughness. The IM7/8552 fracture toughness in Mode II was determined to be 4.11 ± 0.335 in.-lb/in.².

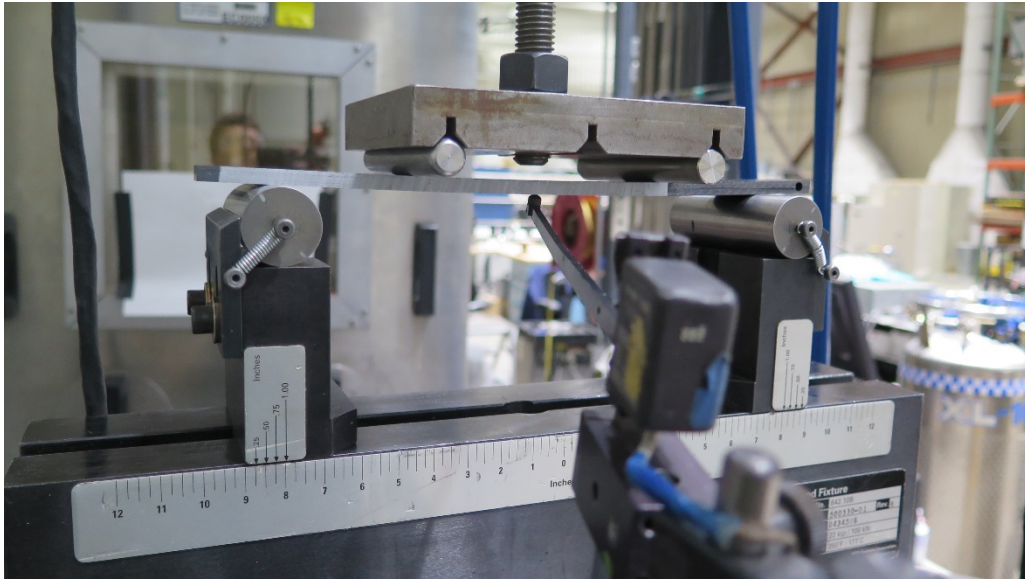


Figure 28.—Test Configuration for Four-Point Bend Testing.

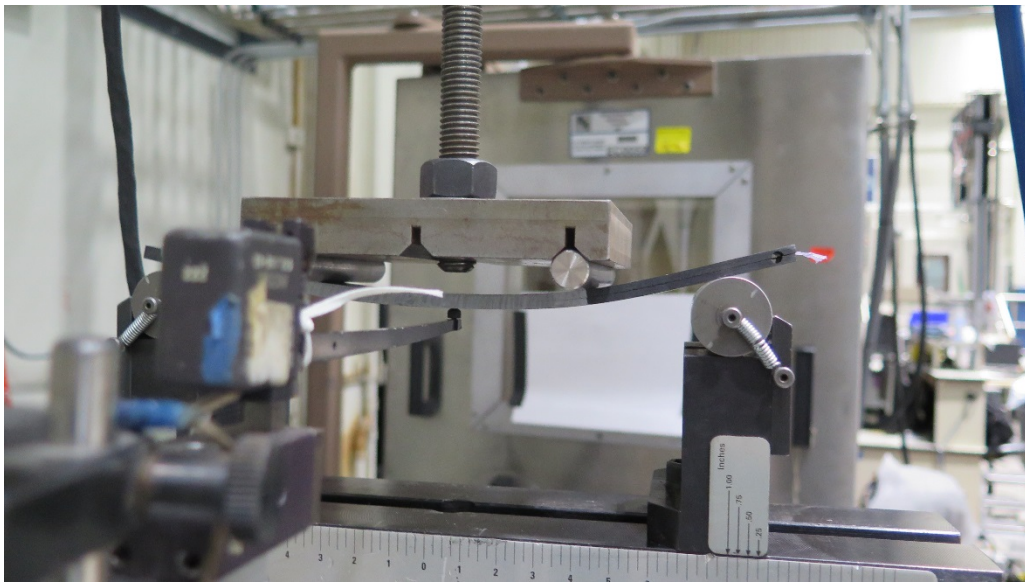


Figure 29.—Failed Sample Subjected to Four-Point Bend Testing.

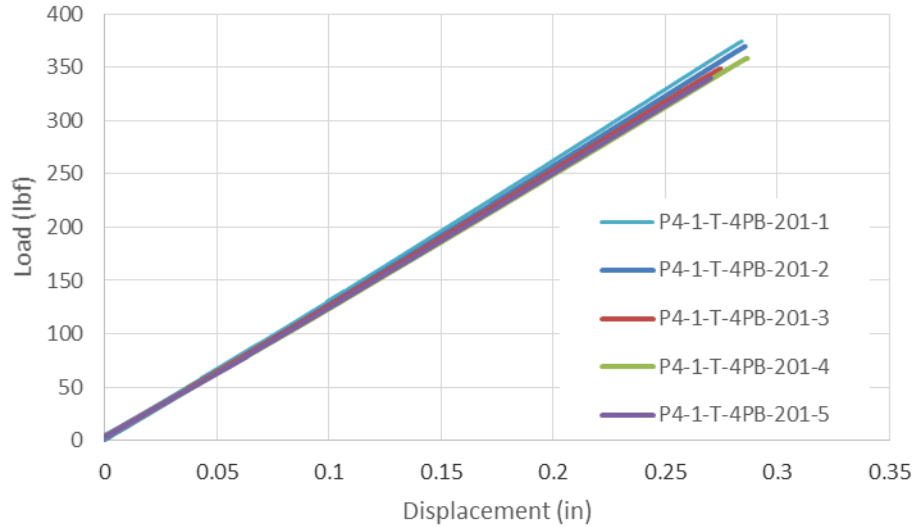


Figure 30.—Load-Deflection Curve for the Four-Point Bend Samples.



Figure 31.—Example of Prepared DCB Specimens with Loading Holes.

4.14 Double Cantilever Beam (DCB)

4.14.1 Testing Details

Samples were cured with a 3 in. Teflon (fluorinated ethylene propylene – FEP) insert placed at the panel midplane to serve as a pre-crack in the panel. Samples were extracted from the bulk panel using a CNC controlled Zimmerman. Samples were inspected and determined to be free of delaminations. The cross-sectional area was measured from the coupon after sample preparation.

Prior to testing, a small hole was cross-drilled into the side of the samples. The hole was drilled 0.5 in. away from the edge of the sample ensuring that the sample had an effective crack length of 2.5 in. per a Boeing internal specification (Figure 31). The inclusion of the hole did not start any additional delaminations. Loading wires are inserted in to the hole and used to apply load to propagate the crack.

4.14.2 Test Results

The energy release rate was determined through data analysis techniques consistent with the energy based approach. The value is determined by establishing the area of the new surface that is generated and the total energy in the system. To calculate the total energy, the instantaneous elastic energy is considered and the following equation is used:

$$\text{Energy} = \sum_{i=1}^n (P_{i+1} - P_i) * L_i$$

To calculate the area of the new surface generated, the length of the crack (a_f) is determined by tracking the crack on the side of the coupon. This length is multiplied by the width (w) of the coupon based on the assumption that the crack front is linear through the width and does not have a curvature. This is shown below.

$$\text{Area} = a_f * w$$

The strain energy release rate can be determined by dividing the total energy by the area. The total equation is shown below:

$$G_{IC} = \frac{\sum_{i=1}^n (P_{i+1} - P_i) * L_i}{a_f * w}$$

Figure 32 shows the load deflection response for the tape coupons. The results are consistent between samples. The tape showed a stable propagation, allowing the determination of a strain energy release rate. The IM7/8552 fracture toughness in Mode I was determined to be 1.85 ± 0.07 in.-lb/in.². Figure 33 shows the failed specimens. From this figure, the crack plane was well defined and no bridging was observed.

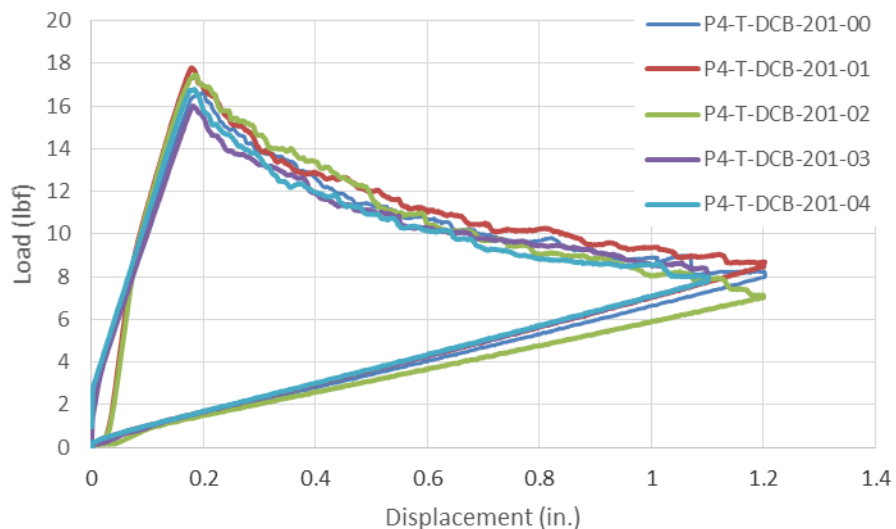


Figure 32.—Load-Deflection Response for Double Cantilevered Beam (DCB) Tests.

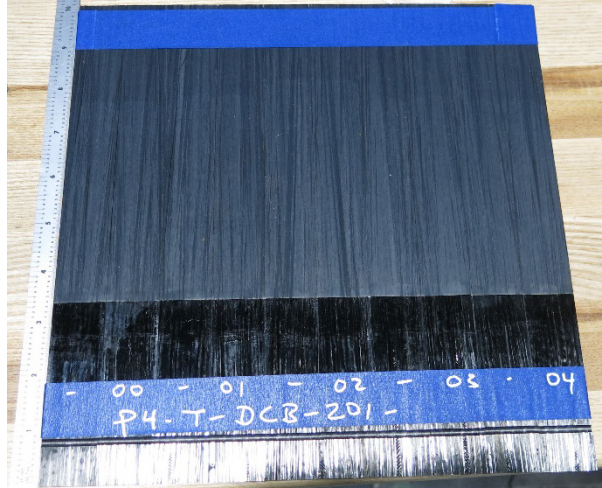


Figure 33.—Failed DCB Specimens of IM7/8552.

4.15 End-Notched Flexure (ENF)

4.15.1 Testing Details

Samples were cured with a 3 in. Teflon insert placed at the panel midplane to serve as a pre-crack in the panel. Samples were extracted from the bulk panel using a diamond coated wet saw. Samples were inspected to be free of delaminations. The cross-sectional area was measured from the coupon after sample preparation.

The test configuration is shown in Figure 34. The bottom rollers had a diameter of 0.25 in. and the bottom two rollers had a diameter of 0.5 in. The test had a total span of 8 in. and was centered in the specimen. The top roller was applied to the center of the specimen with an offset from either end by 2 in.

The sample was loaded under displacement control at a loading rate of 0.002 in./s., the crack was monitored using a microscope, and the location of the crack was noted. Prior to testing, the compliance of the fixture was determined by loading the fixture with an elastic bar. Based on this compliance, the critical load was established. This load was not exceeded for testing as the data becomes unreliable. The crack propagation was monitored throughout the test until the critical load was reached.

4.15.2 Test Results

As part of the pretest setup calibration, the compliance was determined and the critical load was determined to be 160 lb for the tape. The strain energy release rate can be determined in a similar manner as the mode I tests by dividing the total energy by the area. The total equation is shown below:

$$G_{IIc} = \frac{\sum_{i=1}^n (P_{i+1} - P_i) * L_i}{a_f * w}$$

The fracture toughness in Mode II was determined to be 4.44 ± 0.36 in.-lb/in.². Figure 35 shows the load-displacement response. Figure 36 shows the failed samples for the IM7/8552 material system. As seen with the DCB results, the crack stayed in the plane and no bridging was observed in this system.

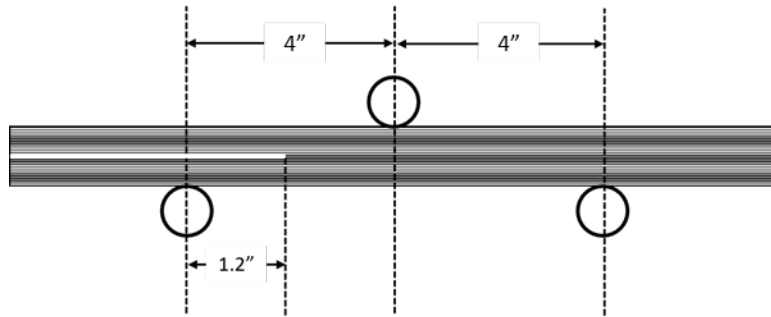


Figure 34.—Test Configuration for ENF Testing.

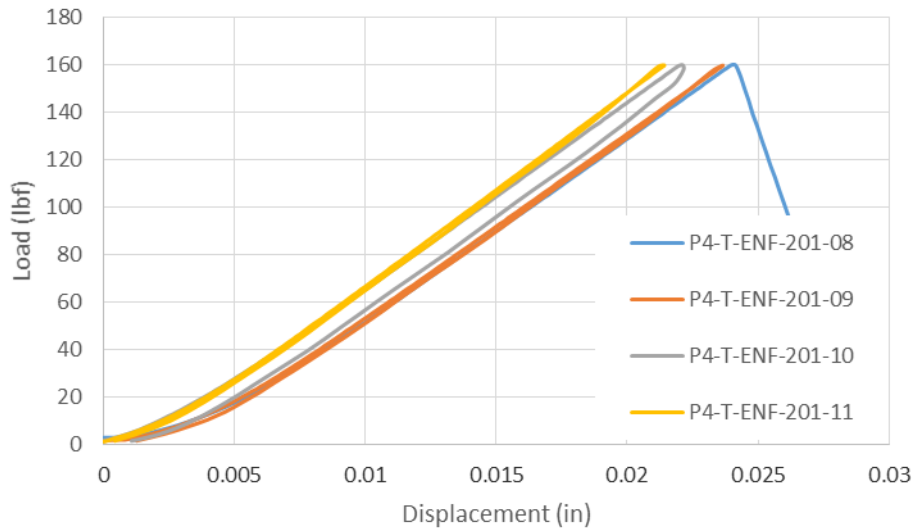


Figure 35.—Load-Deflection Response for End Notch Flexure (ENF) Tests.

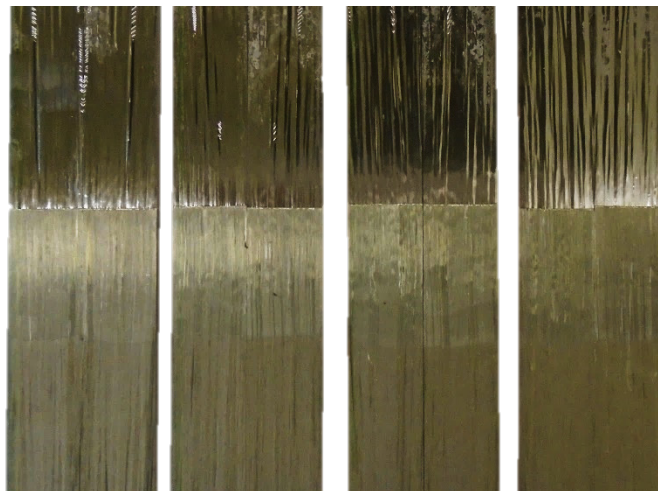


Figure 36.—Failed ENF Specimens of IM7/8552.

4.16 Mixed-Mode Bending (MMB)

4.16.1 Testing Details

Testing was performed by the National Institute for Aviation Research (NIAR) with coupons provided by Boeing. Samples were cured with a 3 in. Teflon insert placed at the panel midplane to serve as a precrack in the panel. Samples were extracted from the bulk panel using a diamond coated wet saw. Samples were inspected to be free of delamination. The cross-sectional area was measured from the coupon after sample preparation.

Upon receiving the coupons, piano hinges were bonded to the samples using FM 300-2 adhesive using a 250 °F cure for 90 min. Testing was performed in accordance with the ASTM D6671 standard. Testing was performed on an MTS electromechanical load frame with a load capacity of 1000 lbf. The displacement was measured using a laser extensometer (Figure 37). The crack tip was monitored using a digital camera with 70x optical zoom.

4.16.2 Test Results

Testing was performed over targeted three mixed mode ratios (MMRs): 25, 50, and 75 percent. In general, five specimens were tested except in the event where there was hinge failure (additional specimens tested). Hinge failure was only observed on the 75 percent mixed mode ratio, and those data are not included in any calculations or figures below. The measured fracture toughness values are shown in Table 15. As the mixed mode ratio increased, the measured fracture toughness increased as well. In general, repeatable results were obtained. This is evidenced by the load-displacement curves for the 25, 50, and 75 mixed mode ratios as shown in Figure 38, Figure 39, and Figure 40, respectively. With a 25 percent mixed mode ratio, crack propagation was initially unstable near a 0.07 in. displacement, but became stable afterwards. For the 50 and 75 percent mixed mode ratios, crack propagation was unstable.

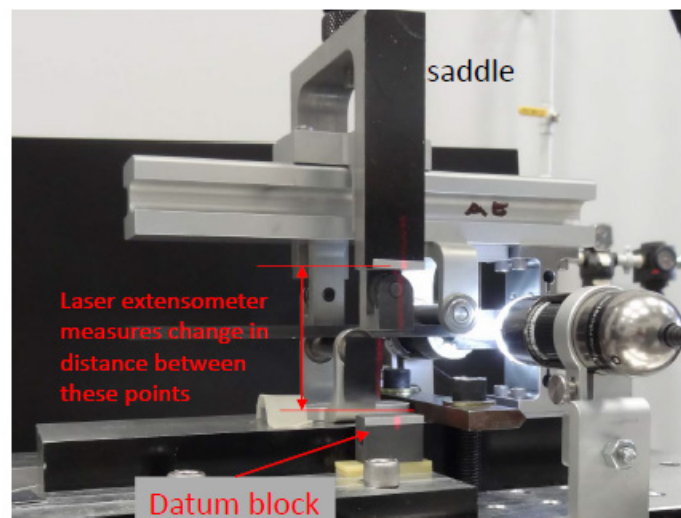


Figure 37.—Test setup for MMB testing.

TABLE 15.—MEASURED FRACTURE TOUGHNESS VALUES FOR MIXED MODE BENDING

Mixed mode ratio, percent	G_c , (lb-in./in. ²)
	Ave. (% c.v.)
25	2.24 (6.0)
50	3.49 (2.2)
75	7.05 (7.6)

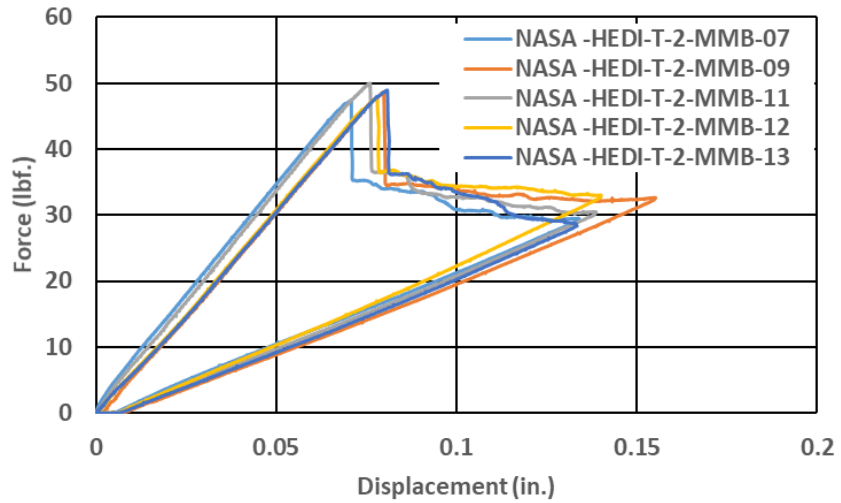


Figure 38.—Load Displacement Curves for a 25 percent Mixed Mode Ratio.

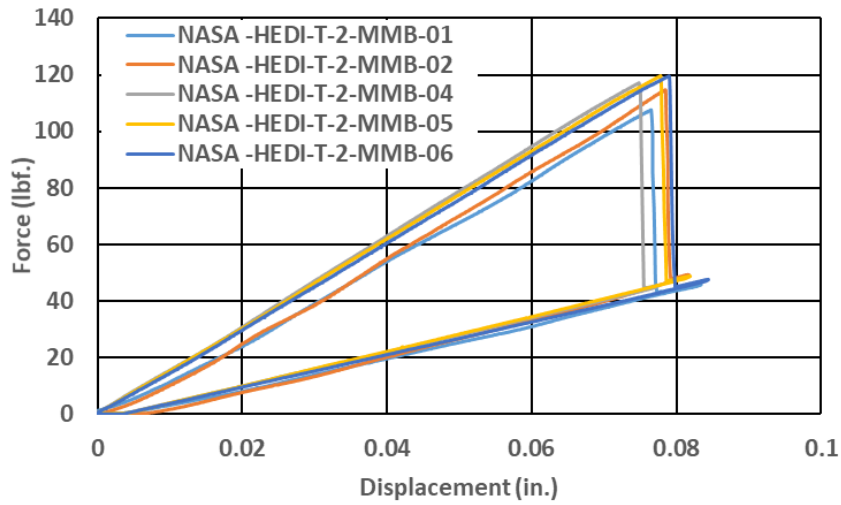


Figure 39.—Load Displacement Curves for a 50 percent Mixed Mode Ratio.

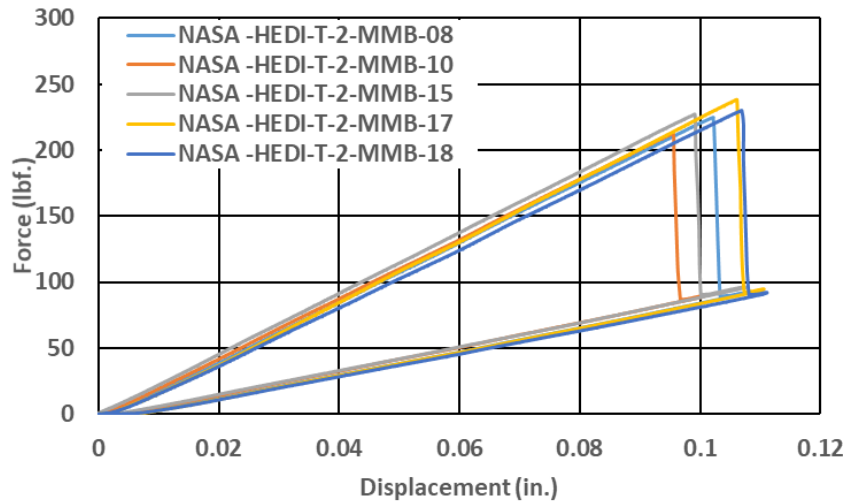


Figure 40.—Load Displacement Curves for a 75 percent Mixed Mode Ratio.

References

1. B. Justusson, J. Pang, M. Molitor, M. Rassaian and R. Rosman, An Overview of the NASA Advanced Composites Consortium High Energy Dynamic Impact Phase II Technical Path, AIAA Scitech 2019 Forum, San Diego, 2019.
2. C. Rose, C. Davila and F. Leone, Analysis Methods for Progressive Damage of Composite Structures, NASA/TM—2013-218024, 2013.
3. Hexply 8552 Product Data, [Online].
Available: https://www.hexcel.com/user_area/content_media/raw/HexPly_8552_us_DataSheet.pdf.
4. LS-DYNA, [Online]. Available: www.lstc.com/products/ls-dyna.
5. H. Razi, J. Schaefer, S. Wanthal, J. Handler, G. Renieri and B. Justusson, Rapid Integration of New Analysis Methods in Production, Thirty-First Technical Conference for The American Society for Composites, Williamsburg, VA, 2015.
6. H. Koerber, High Strain Rate Characterization of Unidirectional Carbon-Epoxy IM7-8552 in Transverse Compression and In-Plane Shear Using Digital Image Correlation, Mechanics of Materials, pp. 1004–1119, 2010.

